The riddle of eastern tropical Pacific ocean oxygen levels : the role of the supply by intermediate depth waters.

Olaf Duteil (oduteil@geomar.de)(1), Ivy Frenger(1), Julia Getzlaff(1)

(1) GEOMAR, Kiel, Germany

Abstract

Observed Oxygen Minimum Zones (OMZs) in the tropical Pacific ocean are located above intermediate depth waters (IDW) defined here as the 500 – 1500 m water depth. Typical climate models do not represent IDW properties and are characterized by a too deep reaching OMZ. We ~~test~~ analyze here the role of the IDW on the misrepresentation of oxygen levels in a heterogeneous subset of ocean models characterized by a horizontal resolution ranging from 0.1° to 2.8°. First, we show that forcing the extra tropical boundaries (30°S/N) to observed oxygen values results in a significant increase of oxygen levels in the intermediate eastern tropical region. Second, the equatorial intermediate current system (EICS) is a key feature connecting the western and eastern part of the basin. Typical climate models lack in representing crucial aspects of this supply at intermediate depth, as the EICS is basically absent in models characterized by a resolution lower than 0.25°. These two aspects add up to a "cascade of biases", that hampers the correct representation of oxygen levels at intermediate depth in the eastern tropical Pacific Ocean and potentially future OMZs projections.

1. Introduction

Oxygen levels in the ocean are characterized by high values in the high latitudes and the subtropical gyres, while concentrations decrease to close to zero in the tropical oceans in the Oxygen Minimum Zones (OMZs). While OMZs are natural features, climate change is potentially responsible for their expansion (Breitburg et al., 2018), leading to a reshaping of the ecosystems and a potential loss of biodiversity.

Modelling oxygen levels is particularly challenging because of the complexity of the interactions between biological processes ~~respiration~~ and physical transport (e.g Deutsch et al., 2014, Ito et al., 2013; Duteil et al., 2014a,b, 2018, Oschlies et al., 2017). Climate models tend to overestimate the volume of the OMZs (Cabre et al., 2015) and do not agree on the intensity and even sign of oxygen future evolution (Oschlies et al., 2017). In order to perform robust projections there is a need to better understand the processes at play that are responsible for the supply of oxygen to the OMZ. We focus here on the Pacific ocean, where large OMZs are located in a depth range from 100 to 900 m (Karstensen et al., 2008; Paulmier and Ruiz-Pino. 2009). Previous modelling studies have shown that the tropical OMZ extension is at least partly controlled by connections with

38 the subtropical ocean (Duteil et al., 2014). In addition, the role of the equatorial undercurrent
39 (Shigemitsu et al., 2017; Duteil et al., 2018; Busecke et al., 2019), of the secondary Southern
40 Subsurface Countercurrent (Montes et al, 2014), of the interior eddy activity (Frenger et al., 2018),
41 have been previously highlighted. These studies focus on the mechanisms at play in the upper
42 oxygen levels (upper 500 m meter) 500 m of the water column. The oxygen content below the core
43 of the OMZ however plays a significant role in setting the upper oxygen levels by diffusive (Duteil
44 and Oschlies, 2009) or vertical advective (Duteil, 2019) processes. Here, we focus specifically on
45 the mechanisms supplying oxygen toward the eastern tropical pacific ocean at intermediate depth
46 (500 – 1500 m), below the OMZ core.

47

48 The water masses occupying this intermediate depth layer (500 – 1500 m) (Emery, 2003) subduct
49 at high latitudes. (Karstensen et al., 2008). Oxygen solubility increases with lower temperatures,
50 thus waters formed in the Southern Ocean and in the North Pacific are characterized by high
51 oxygen values. In particular, the Antarctic Intermediate Water (AAIW) (Molinelli, 1981) ventilates
52 large areas of the lower thermocline of the Pacific Ocean (Sloyan and Rintoul., 2001) and is
53 characterized by oxygen values larger than 300 mmol.m^{-3} at subduction time (Russel and Dickson,
54 2003). The oxygenated core of the AAIW in the tropical Pacific is located at about 500-1200 m
55 depth at 40°S (Russell and Dickson, 2003) and with this at a depth directly below the depth of the
56 OMZs in the eastern Pacific; the Pacific AAIW mixes down to 2000 m depth with the oxygen poor
57 Pacific Deep Water (PDW) as determined by the OMP (Optimum Multiparameter) analysis (Pardo
58 et al., 2012; Carrasco et al., 2017). The oxygen rich (> 200 mmol.m^{-3} at 40°S) AAIW spreads from
59 its formation side in the Southern Ocean to the subtropical regions. The northern part of the Pacific
60 basin is characterized by the North Pacific Intermediate Water (NPIW) (Talley, 1993) confined to
61 the northern Pacific conversely to the AAIW, which spreads far northward as its signature reaches
62 15°N (Qu and Lindstrom., 2004). AAIW, NPIW and the upper part of the PDW are oxygenated
63 water masses occupying the lower thermocline between 500 and 1500 m depth.In this study we do
64 not specifically focus on the individual water masses, but rather on the water occupying the
65 intermediate water depth (500 – 1500 m) (Emery, 2003) of the subtropical and tropical ocean. We
66 will refer to the waters in this depth range as intermediate depth waters (IDW).

67

68 In the subtropics, the IDW (particularly the AAIW) circulates into the intermediate flow of the South
69 Equatorial Current and the New Guinea Coastal Undercurrent (Qu and Lindstrom, 2004) where it
70 retroflects in the zonal equatorial flows of the Southern Intermediate Countercurrent (SICC) and
71 Northern Equatorial Intermediate Current (NEIC) within about ±2° off the equator (Zenk et al.,
72 2005; Kawabe et al., 2010) (Fig 1). These currents are part of the Equatorial Intermediate Current
73 System (EICS) constituted by a complex system of narrow jets extending below 500 m in the lower
74 thermocline (Firing, 1987; Ascani et al., 2010; Marin et al. 2010; Cravatte et al., 2012, 2017;

Menesguen et al., 2019). While the existence of this complex jet system has been shown to exist in particular using argo floats displacements (Cravatte et al., 2017) the spatial structure and variability of the jets are still largely unknown. In addition, there is little knowledge about their role in transporting properties such as oxygen.

The simulation of the supply of oxygen to the eastern tropical Pacific below the OMZ core is a difficult task as it depends on the realistic simulation of the IDW ~~~properties (in particular the oxygen content) and the IDW pathway (through the EICS). It is known that current climate models, in particular CMIP5 (Coupled Model Intercomparison Project phase 5) models, have deficiencies in correctly representing the IDW~~They generally display , and in particular the AAIW.~~ In particular, the AAIW is too shallow and thin ~~IDW~~, with a limited equatorward extension compared to observations (Sloyan and Kamenkovich, 2007; Sallee et al., 2013; Meijers, 2014; Cabre et al., 2015; Zhu et al., 2018 for the south Atlantic ocean). Discrepancies in the simulated properties of IDW compared to observations are due to a combination of a range of errors in the climate models, including in the simulation of wind and buoyancy forcing, an inadequate representation of subgrid-scale mixing processes in the Southern Ocean, and midlatitude diapycnal mixing parameterizations (Sloyan and Kamakovich, 2007; Zhu et al., 2018). In addition, the EICS is mostly lacking in coarse resolution models (Dietze and Loeptien, 2013; Getzlaff and Dietze, 2013). Higher resolution (0.25°, 1/12°) configurations partly resolve the EICS but with smaller current speeds than observed (Eden and Dengler, 2008; Ascani et al., 2015). The mechanisms forcing the EICS are complex and still under debate (see the review by Menesguen et al., 2019).

In this study we focus on the role ~~impact~~ of the subtropical and westenr tropical IDW (and of the deficiencies in the representation of its ~~their~~ properties and transport) on the oxygen content in the eastern tropical Pacific in a set of model simulations. Section 2 gives an overview of all models that we used as well as of the sensitivity simulations. Next, we assess to which extent the IDW modulate (or drive) the oxygen levels in the eastern tropical (20°S – 20°N; 160°W-coast) Pacific ocean ~~in this set of models, and determine. The role of the IDW depends i)~~ and determine the role of i) ~~on~~ the oxygen content of the IDW in ~~the lower thermocline of~~ the subtropical regions (section 3) and ii) ~~on~~ the zonal recirculation of the oxygen by the EICS toward the eastern part of the basin (section 4). We conclude in section 5.

2. ~~Analyzed models~~ Description of models and experiments

2.1 Description of models

~~Mean state12.~~

We analyze the mean state of the oxygen fields, OMZ, EICS of the following model experiments (see Table 1), which previously have been used in recent studies focusing on the understanding of the tropical oxygen levels mean state or variability :

(NEMO2 configuration). The circulation model is coupled to a simple NPZD (Nutrient Phytoplankton Zooplankton Detritus) biogeochemical model that comprises 6 compartments (e.g used in Duteil et al., 2018; Duteil, 2019).The simulation has been forced by climatological forcings based on the Coordinated Reference Experiments (CORE) v2 reanalysis (Normal Year Forcing) (Large and Yeager, 2009) and integrated for 1000 years. - the NEMO (Nucleus for European Modelling of the Ocean) model (Madec et al., 2017) with a resolution of 2°, refined meridionally to 0.5° in the equatorial region

- The NEMO (Nucleus for European Modelling of the Ocean) model (Madec et al., 2017) has been used throughout this study in different configurations. We first use a coarse resolution version (see 2.2). This configuration is known in the literature as ORCA2 (Madec et al., 2017) but we call it NEMO2 in this study for clarity reasons. The resolution is 2°, refined meridionally to 0.5° in the equatorial region. It possesses 31 vertical levels on the vertical (10 levels in the upper 100 m), ranging from 10 m to 500 m at depth. Advection is performed using a third-order scheme. Isopycnal diffusion is represented by a biharmonic scheme along isopycnal surfaces. The parameterisation of Gent and McWilliams (1990) (hereafter GM) has been used to mimic the effect of unresolved mesoscale eddies. The circulation model is coupled to a simple biogeochemical model that comprises 6 compartments (phosphate, phytoplankton, zooplankton, particulate and dissolved organic matter, oxygen). The same configuration has been used in Duteil et al., 2018; Duteil, 2019. The simulation has been forced by climatological forcings based on the Coordinated Reference Experiments (CORE) v2 reanalysis (Normal Year Forcing) (Large and Yeager, 2009) and integrated for 1000 years. Initial fields (temperature, salinity, phosphate, oxygen) are provided by the World Ocean Atlas 2018 (WOA) (Garcia et al, 2019; Locarnini et al., 2019)

Two other versions of NEMO have been used (see 2.2). The configuration ORCA05 (that we call here NEMO05) is characterized by a spatial resolution of 0.5°. It possesses 46 levels on the vertical, ranging from 6 to 250 m at depth (15 levels in the upper 100 m). Advection is performed using a third-order scheme. Isopycnal diffusion is represented by a biharmonic scheme along isopycnal surfaces. Effects of unresolved mesoscale eddies are parameterized following GM. In the configuration TROPAC01 (that we call NEMO01 in the rest of this study), a 0.1° resolution two-way AGRIF (Adaptive Grid Refinement In Fortran) has been embedded between in the Pacific Ocean into the global NEMO05 grid (similar to the configuration used in Czeschel et al., 2011). Since the model is eddying in the nested region GM is not used. Both configurations are forced by the same interannually varying atmospheric data given by the Coordinated Ocean–Ice Reference Experiments (CORE) v2 reanalysis products over the period 1948–2007 (Large and Yeager,

- the UVIC (University of Victoria) model (e.g used in Getzlaff et al., 2016; Oschlies et al., 2017), an earth System Model (ESM) that has a horizontal resolution of 1.8° latitude x 3.6° longitude. The experiment has been integrated for 10000 years. The biogeochemical model is a NPZD-type model of intermediate complexity that describes the full carbon cycle (see Keller et al., 2012 for a detailed description). This model is forced by monthly climatological NCAR/NCEP wind stress fields.

- the GFDL (Geophysical Fluid Dynamics Laboratory) CM2-0 suite (Delworth et al., 2012; Griffies et al., 2015, Dufour et al, 2015): the suite is based on the GFDL global climate model and includes a fully coupled atmosphere with a resolution of approximately 50 km. It consists of three configurations that differ in their ocean horizontal resolutions: GFDL1 (original name : CM2-1deg) with a nominal 1° resolution, GFDL025 (original name : CM2.5) with a nominal 0.25° and GFDL01 with a nominal 0.1° resolution (original name : CM2.6)(e.g These configurations have been used in Frenger et al., 2018 and Busecke et al., 2019 for studies on ocean oxygen). At simulation year 48, the simplified ocean biogeochemistry model miniBLING is coupled to the models, with three prognostic tracers, phosphate, dissolved inorganic carbon and oxygen (Galbraith et al., 2015). Due to the high resolution of GFDL01, the integration time is limited. We here analyze simulation years 186 to 190.

All the models (NEMO2, UVIC, GFDL suite) are forced using preindustrial atmospheric pCO_2 concentrations.

Differences in model resolution but also in atmosphere forcings or spinup duration strongly impact oxygen distribution (see Annex A). However, the heterogeneity of the configurations that we analyze permits to determine whether the simulated oxygen distributions display systematic biases / similar patterns.

The mean states of the oxygen distributions are discussed below in section 3.1 "IDW Oxygen levels in models".

2.2 Sensitivity experiments

In order to disentangle the different processes at play, we perform two different sets of sensitivity simulations, using the NEMO model engine. NEMO allows to test effects of increasing the ocean resolution and to integrate the model over a relatively long time span.

 Sensitivity simulations

In order to disentangle the different processes at play we perform two different sets of sensitivity simulations using the NEMO model engine. NEMO allows to test effects of increasing the ocean resolution and to integrate the model over a relatively long time span. All sensitivity experiments are integrated for 60 years (1948 to 2007) using the CORE (Coordinated Ocean-Ice Reference Experiments) v2 interannual (Large and Yeager, 2009) forcings. This time scale permits the recirculation from the interior subtropical regions to the tropical area (as suggested in the model study by SenGupta and England, 2007).22.

2.2.1 Forcing of oxygen to observed values in the subtropical regions

In the first set of experiments the focus is on the role of the lower thermocline oxygen content for the ventilation of the eastern equatorial Pacific. We use NEMO2, the oceanic component of the IPSL-CM5A (Mignot et al., 2013), that is part of CMIP5. NEMO2 shows mid-latitudes oxygen biases consistent with CMIP5 models. We compare three experiments :

- NEMO2-REF: the experiment is integrated from 1948 to 2007 starting from the spinup state described in 2.1.

- NEMO2-30S30N: the oxygen boundaries are forced to observed oxygen concentrations (WOA) at the boundaries 30°N and 30°S in the whole water column: the mid-latitude oxygen levels in the IDW are therefore correctly represented.

- NEMO2-30S30N1500M: same as NEMO2-30S30N; in addition oxygen is forced to observed concentrations at the depth interface of below 1500m, mimicking a correct oxygen state of the deeper water masses (lower part of the AAIW, upper part of the PDW)

With the above three experiments we focus on the transport of IDW oxygen levels to the tropical ocean and the OMZs. The respiration rate (oxygen consumption) is identical in NEMO2-REF, NEMO2-30S30N and NEMO2-30S30N1500M in order to avoid compensating effects between supply and respiration that depend on biogeochemical parameterizations (e.g Duteil et al., 2012). We aim to avoid such compensating effects to ease interpretation and be able to focus on the role of the physical transport. The sensitivity of tropical IDW oxygen to subtropical and deep oxygen levels is discussed in section 3.2

2.2.2 Conservative Tracer Release in oxygenated waters

In the a second set of experiments, we assessed the effect of a resolution increase on the transport of a conservative tracer. To do this, we used a 0.5° (NEMO05) and a higher resolution 0.1° (NEMO01) configuration of the NEMO model engine (Table 1) to examine the transport of oxygenated IDW from the subtropical regions into the oxygen deficient tropics.NEMO01 is a configuration based on NEMO05 and where a 0.1° two-ways nest has been embedded in the

221 whole Pacific Ocean, from 49°S to 31°N (Czeschel et al, 2011). In these experiments, we
222 initialized the regions with climatological (WOA) oxygen levels greater than 150 mmol.m^{-3} with a
223 value of 1 (and 0 when oxygen was lower than 150 mmol.m^{-3}). In the model simulations, the tracer
224 is subject to the same physical processes as other physical and biogeochemical tracers, i.e.
225 advection and diffusion but it does not have any sources and sinks. The experiments have been
226 integrated for 60 years (1948 – 2007) using realistic atmospheric forcing (COREv2). NEMO05 and
227 NEMO01 display a similar upper ocean circulation (Fig 5) but NEMO05 does not simulate a
228 developed EICS in contrast to NEMO01.

229

230 In order to complement the tracer experiment we performed Lagrangian particle releases.
231 Lagrangian particles allow to trace the pathways of water parcels due to the resolved currents, and
232 to track the origin and fate of water parcels. They are not affected by subgrid scale diffusive and
233 advective processes. The particles are advected offline with 5 days mean of the NEMO05 and
234 NEMO01 currents. The NEMO01 circulation fields have been interpolated to the NEMO05 grid in
235 order to allow a comparison of the large scale advective patterns between NEMO01 and
236 NEMO05. We do not take into account subgrid processes in NEMO05. We used the ARIANE tool
237 (Blanke and Raynaud, 1997). A first particle release has been performed in the eastern tropical
238 OMZ at 100°W in the tropical region between 105°S – 105°N., a second release has been
239 performed in the western part of the basin at 160°E. The particles have been released in the IDW
240 lower thermocline at (51000 - 1500 m) and integrated backward in time from 2007 to 1948 in order
241 to determine their pathways and their location of origin. We released 120 particles every 5 days
242 during the last year of the experiment, for a total of 8760 particles. The transport by the EICS is
243 discussed in section 4.2 (tracers levels and Lagrangian pathways).

244

245 **3. Intermediate water properties and oxygen content**
246 3.1. IDW Oxygen levels in models
247 The water masses IDW subducted in mid/high latitudes are highly oxygenated waters. As part of
248 the deficient representation of IDW, tThe subducted "oxygen tongue" (oxygen values up to 240
249 mmol.m^{-3}) located at IDW level is not reproduced in most of the models part of CMIP5 (Fig 8 from
250 Cabre et al., 2015, Fig 4 from Takano et al., 2018) and in the models analyzed here (Fig 2a), with
251 an underestimation of about 20-60 mmol.m^{-3} (NEMO2, GFDL1, GFDL025, GFDL01). UVIC, a
252 coarse resolution model, shows oxygenated waters in the lower thermocline at mid latitudes (30°S-
253 50°S); the oxygenation however likely arises due to a too large vertical diffusion from the mixed
254 layer rather than by an accurate representation of the water masses.

255

256 GFDL01, even though still biased low, presents larger oxygen values than the coarser resolution
257 models GFDL1, GFDL025 and NEMO2. A possible explanation is a better representation of the
258 water masses and in particular the AAIW in eddy-resolving models (Lackhar et al., 2009).

259

260 The IDW oxygen maximum is apparent at 30°S throughout the lower thermocline (600 – 1000 m) in
261 observations (Fig 2b), consistent with the circulation of IDW with the gyre from the mid/high latitude
262 formation regions towards the northwest in subtropical latitudes (Sloyand and Rintoul. 2001), and
263 followed by a deflection of the waters in the tropics towards the eastern basin (Qu et al., 2004;
264 Zenk et al., 2005). This oxygen peak is missing in all the models analyzed here.

265

266 Consistent with the low oxygen bias of models at subtropical latitudes (Fig 2b), models also feature
267 a bias in the tropical ocean (20°S-20°N) by 20 – 50 $mmol.m^{-3}$ (Fig 2a, Fig 2c) at intermediate
268 depths in the eastern part of the basin (similarly to CMIP5 models, as shown by Cabre et al.,
269 2015). The basin zonal average of the mean oxygen level in the lower thermocline layer (500 -
270 1500m) at 30°S and in the eastern part of the basin (average 20°S – 20°N, 160°W-coast; 500-1500
271 m) are positively correlated (Pearson correlation coefficient R=0.73) (Fig 2d, Annex A), suggesting
272 that the oxygen levels in the tropical pacific ocean are partly controlled by extra-tropical oxygen
273 concentrations at intermediate depths and the associated water masses.

274

275 The models presenting the poorest oxygenated water at 30°S display the largest volume of OMZs
276 (GFDL025 and GFDL1), though the negative correlation (Pearson correlation coefficient R=-0.52)
277 is less pronounced between the volume of the OMZs and the mean oxygen levels in the layer 500 -
278 1500 m at 30°S (Fig 2e). A correlation, even weak, suggests a major role of the IDW in regulating
279 the OMZ volume. Reasons for this weaker correlation are due to the OMZs being a result of
280 several processes next to oxygen supply by IDW, e.g, vertical mixing with other water masses
281 (Duteil et al., 2011), isopycnal mixing in the upper thermocline (Gnanadesikan et al., 2013; Bahl et
282 al., 2019), supply by the upper thermocline circulation (Shigemitsu et al., 2017; Busecke et al.,
283 2019). A correlation, even weak, suggests a major role of the IDW in regulating the OMZ volume.

284

285 In order to better understand the role of IDW entering the subtropical domain from higher latitudes
286 for the oxygen levels in the eastern tropical Pacific Ocean, we perform sensitivity experiments (see
287 2.2.1) in the following.

288

289 3.2 Sensitivity of tropical IDW oxygen to subtropical and deep oxygen levels
290 3.2.1 Oxygen levels in the lower thermocline

291   The difference of the experiments NEMO2-30S30N – NEMO2-REF (average 1997-2007) (Fig 3c,d)

292   allows to quantify the effect of model biases of IDW at mid latitudes (30°N/30°S) on tropical oxygen

293   levels.

294

295   We first assess the oxygen concentration and density levels at 30°S and 30°N in both the World

296   Ocean Atlas (WOA) and the NEMO2-REF experiment. The deficiency in oxygen in NEMO2-REF is

297   clearly highlighted at 30°S, between 400 and 1500m. The density levels are well reproduced in

298   NEMO2-REF compared to WOA (Annex B).

299

300

301

302   As we force restore oxygen to observed levels at 30°S/°N (see 2.2.1), the difference between both

303   experiments shows a large anomaly in oxygen levels at 30°S (more than 50 mmol.m^{-3}) at lower

304   thermocline level (500 – 1500 m) corresponding to the missing deep oxygen maximum, located in

305   the IDW. The northern negative anomaly results from a deficient representation of the north Pacific

306   OMZ, i.e., modeled oxygen is too high for NPIW. The northern low and southern high anomalies

307   spread towards the tropics at intermediate depth. A fraction of the positive oxygen anomaly

308   recirculates at upper thermocline level due to a combination of upwelling and zonal advection by

309   the tropical current system (for instance the EUC at thermocline level is a major supplier of oxygen

310   as shown in observations by Stramma et al., 2010 and in ocean models by Duteil et al., 2014,

311   Busecke et al., 2019).

312

313   The difference NEMO2-30S30N1500M – NEMO2-30S30N (Fig 3e,f) shows a deep positive

314   anomaly in oxygen, as oxygen levels are lower than in observations by 30-40 mmol.m^{-3} in the

315   eastern tropical regions. This anomaly is partially transported into the IDW (500 - 1500 m). It shows

316   that a proper representation of the deep oxygen levels (> 1500 m) is important for a realistic

317   representation of the lower thermocline and OMZs. Causes of the oxygen bias of the deeper water

318   masses are beyond the scope of this study but may be associated with regional (tropical) issues,

319   such as an improper parameterization of respiration (e.g a too deep remineralisation) (Kriest et al.,

320   2010), or a misrepresentation of deeper water masses.

321

322   3.2.2 Oxygen budget and processes

323   To assess the processes that drive the oxygen content of the (sub)tropical lower thermocline, we

324   analyzed the oxygen budget in NEMO2-REF and NEMO2-30S30N, NEMO30S30N1500M. The

325   budget is computed as an average between 500 and 1500m and shown in Fig 3g and Fig.4.

326

327   The oxygen budget is :

9   9

$$328 \quad \frac{\delta O_2}{\delta dt} = Adv_x + Adv_y + Adv_z + Diff_{Dia} + Diff_{Iso} + SMS$$

329   where Adv_x, Adv_y, Adv_z, are respectively the zonal, meridional and vertical advection terms, $Diff_{dia}$

330   and $Diff_{iso}$ are the diapycnal and isopycnal diffusion terms. SMS (Source Minus Sink) is the

331   biogeochemical component (i.e below the euphotic zone this is only respiration)

332

333   In NEMO2-REF, the physical oxygen supply is balanced by the respiration. The oxygen supply in

334   the model is divided into advection, i.e., oxygen transport associated with volume transport, and

335   isopycnal diffusion, i.e., subgrid scale mixing processes that homogenize oxygen gradients (Fig

336   4a). Diapycnal diffusion is comparatively small and can be neglected.

337

338   The supply of oxygen from the high latitudes toward the tropical interior ocean is constituted by

339   several processes acting concomitantly : isopycnal diffusion transfers oxygen from the oxygen-rich

340   gyres to the poor oxygenated regions (see Fig 1). ~~The lower branches of~~ Below the subtropical

341   gyre~~, s transport the~~ the oxygen is transported from the western to the eastern ~~eastern to the~~

342   ~~western~~ part of the basin. Downwelling from the oxygen-rich mixed layer supplies the interior of the

343   subtropical gyre~~s~~. At the equator, the EICS transport westward oxygen-poor water originating in

344   the eastern side of the basin (Fig 4a). The meridional advection term transports oxygen originating

345   from the subtropics in the tropical regions, which is upwelled.

346

347   Forcing oxygen levels in NEMO2-30S30N at 30°S and 30°N creates an imbalance between

348   respiration (which remains identical in NEMO2-REF and NEMO2-30S30N) and supply. The oxygen

349   anomaly generated at 30°S propagates equatorward. The positive anomaly originated from the

350   southern boundary recirculates in the equatorial region. Isopycnal diffusion is a major process that

351   transport the oxygen anomaly toward the equator (Fig 3g, Fig 4b), in particular from 30°S to the

352   5°S and 30°N to 10°N. Total advective transport plays an important role in the transport of the

353   oxygen anomaly as well, especially in the equator region and in the western boundary currents.

354   Meridional advection plays a large role close to the 30° boundaries as the oxygen is transported by

355   the deeper part of the gyres. As the vertical gradient of oxygen decreases (the intermediate ocean

356   being more oxygenated), the vertical supply from the upper ocean decreases in the south

357   (increases in the north) subtropical gyre. Comparatively the impact on zonal term advection is

358   small as the zonal oxygen gradient stays nearly identical in both experiments (the oxygen anomaly

359   is almost longitude independent). The model does not display much increase in zonal recirculation

360   at the equator as well, except in the western part of the basin due to the advection of the oxygen

361   provided by the retroflection of the deep limb of the subtropical gyre. The increase of meridional

362   transport is caused by the change in oxygen meridional gradient, mainly caused by isopycnal

363   diffusion processes away from the western boundary.

364 ~~s the vertical gradient of oxygen decreases (the intermediate ocean being more oxygenated), the~~
365 ~~vertical supply from the upper ocean decreases in the south (increases in the north) subtropical~~
366 ~~gyre and decreases at the equator (Fig 4b). The meridional oxygen gradient between the southern~~
367 ~~subtropical gyre and the equator strengthens, and so does the meridional transport from the~~
368 ~~subtropics to the equator, partly by the western boundary currents. The changes in zonal transport~~
369 ~~are comparatively small.a Changes in the advective terms are found along the equator: increase~~
370 ~~(south) or decrease (north) of isopycnal diffusion (Fig 3g, Fig 4b.by an Forcing oxygen levels in~~
371 ~~NEMO2-30S30N at 30°S and 30°N creates an imbalance between respiration (which remains~~
372 ~~identical in NEMO2-REF and NEMO2-30S30N) and supply. This imbalance is most apparent in the~~
373 ~~tropics~~

375 In the experiment NEMO2-30S30N1500, in complement to the isopycnal propagation of the
376 subtropical anomaly, the deep (> 1500 m) oxygen anomaly is upwelled in the eastern equatorial
377 (500 – 1500 m) part of the basin (see Fig 3g). The transport due to advective terms strongly
378 increases, mostly due to an increase in vertical advection. This is consistent with the analysis by
379 Duteil (2019) who showed that vertical advection is the dominant process to supply oxygen from
380 the lower to the upper thermocline in the equatorial eastern Pacific Ocean in a similar NEMO2
381 configuration.

383 This simple set of experiments already shows that in climate models oxygen in the lower
384 thermocline (500 – 1500 m) tropical ocean are partially controlled by properties of IDW that enter
385 the tropics from higher latitudes. This presumably also applies to other (biogeochemical) tracers.
386 IDW oxygen propagates equatorward mostly by small scale isopycnal processes and the western
387 boundary currents. Further, upwelling in the tropics from deeper ocean layers (Pacific Deep Water,
388 partially mixed with the lower IDW) play an important role. We will examine more closely in the
389 following the representation and the role of the EICS in supplying oxygen toward the eastern
390 Pacific Ocean.

392 **4. Equatorial intermediate current system and oxygen transport**
393 4.1 Structure of the currents in the upper 2000 m in observations and models
394 The current structure of the models analyzed in this study (see section 2.1, Table 1) is shown in
395 Fig 5. In the mixed layer, the broad westward drifting South and North Equatorial Currents (SEC,
396 NEC) characterize the equatorial side of subtropical gyres. In the thermocline, the eastward flowing
397 equatorial undercurrent (EUC), flanked by the westward flowing south and north counter currents
398 are present in all models. This upper current structure is well reproduced (i.e the spatial structure
399 and intensity are consistent with observations) across the different models (see 2.1 "Model
400 analyzed") compared to observations. Previous studies already discussed the upper thermocline

401 current structure in the GFDL models suite (Busecke et al., 2019), NEMO2 and NEMO05 (e.g

402 Izumo, 2005, Lübbecke et al., 2008), UVIC (Loeptien and Dietze, 2013); the upper thermocline will

403 not be further discussed in this study.

404

405 At intermediate depth, in the observations, a relatively strong (about 0.1 ms^{-1}) westward flowing

406 Equatorial Intermediate Current (EIC) is present below the EUC at about 400-600 m depth (Marin

407 et al., 2010). A complex structure of narrow and vertically alternating jets every 200 m, so-called

408 Equatorial Deep Jets (EDJ), extends below the EIC till 2000 m (Firing, 1987; Cravatte et al., 2012).

409 Laterally to the EIC, in the upper thermocline, the Low Latitude Subsurface Countercurrents

410 (LLSC) are observed. They include the North and South Subsurface Counter Currents (NSCC and

411 SSCC), located around 5°N/5°S, and a series of jets between 5°N/S and 15°N/S (in particular the

412 Tsuchiya jets in the southern hemisphere, described by Rowe et al., 2000). Below the LLSCs, the

413 Low Latitude Intermediate Currents (LLICs) include a series of westward and eastward zonal jets

414 (500–1500-m depth range) alternating meridionally from 3°S to 3°N; the North and South

415 Intermediate Countercurrents (NICC and SICC) flow eastward at 1.5°–2° on both flanks of the

416 lower EIC. The North and South Equatorial Intermediate Currents (NEIC and SEIC) flow westward

417 at about 3° (Firing, 1987). A detailed schematic view of the tropical intermediate circulation is

418 shown in a recent review by Menesguen et al. (2019) and in Fig 1.

419

420 In coarse resolution models, the intermediate current system is not developed and sluggish (even

421 missing in UVIC and GFDL1). NEMO2 and NEMO05 display ~~a "primitive"~~ an incomplete EICS as

422 the LLSCs are not represented. High resolution models (GFDL025, GFDL01, NEMO01) display a

423 more realistic picture, even if the mean velocity is still weaker than in observations (smaller than 5

424 cm.s^{-1}), where it reaches more than 10 cm^{-1} at 1000 m (Ascani et al., 2010; Cravatte et al., 2017).

425 An interesting feature is that the jets are broader and faster in NEMO01 than in GFDL01. Possible

426 causes include a different wind forcing, mixing strength or topographic features as all these

427 processes play a role in forcing the intermediate jets (see the review by Menesguen et al., 2019).

428 The intermediate currents are less coherent vertically in NEMO01 than in GFDL01, due to their

429 large temporal variability in NEMO01. A strong seasonal and interannual variability of the EICS has

430 been observed that displays varying amplitudes and somewhat positions of the main currents/jets

431 (Firing, 1998; Gouriou et al., 2006: Cravatte et al., 2017). A clear observational picture of the EICS

432 variability is however not yet available. Outside the tropics (in particular south of 15°S), the interior

433 velocity pattern is similar in coarse and high resolution models, suggesting a similar equatorward

434 current transport at intermediate depth in the subtropics, in for instance NEMO05 and NEMO01.

435

436 4.2 Transport by the EICS

437 4.2.1 Tracer spreading towards the eastern tropical Pacific

We released a conservative tracer in the subtropical domain in well oxygenated waters (waters where observed oxygen concentration is greater than 150 mmol.m^{-3} - see 2.2.2) in a coarse (NEMO05) and a high resolution configuration (NEMO01). The tracer does not have sources or sinks and is advected and mixed as any other model tracer and allows to assess the transport pathway of tracer (such as oxygen) from oxygenated waters into the oxygen deficient eastern tropical Pacific.

The importance of the ventilation by the oxygen rich waters, and in particular the IDW, is illustrated by the tropical tracer concentration after 50 years (Fig 6a) of integration (mean 2002-2007). Concentrations decrease from the release location to the northern part of the basin, where the lowest values (below 0.1) are located in NEMO05 and NEMO01. The 0.1 isoline is however located close to the equator in NEMO05 while it is found around 7°N in NEMO01. This feature is associated with a pronounced tongue of high tracer concentration (> 0.2) between 5°N and 5°S in NEMO1. Such a tongue is absent in NEMO05. The enhanced tracer concentration in the equatorial region suggests a stronger zonal equatorial ventilation in NEMO01, consistent with a stronger .EICS (Figure 5)-

The preferential pathways of transport are highlighted by the determination of the transit time it takes for the tracer to spread from the oxygen rich regions to the tropical regions. We define a threshold called t10% when the tracer reaches a concentration of 0.1 (Fig 6b) (similar to the approach of SenGupta and England, 2007). t10% highlights a faster ventilation of the equatorial regions in NEMO01 compared to NEMO05, as t10% displays a maximum value of 10 (western part) to 30 years (eastern part) between 5°N/5°S in NEMO01 compared to 30 years to more than 50 years in NEMO05. The southern "shadow zone" is well individualized in NEMO01 compared to NEMO05 as the oxygen levels are high in the equator in NEMO01, suggesting a strong transport by the EICS. The value of t10% increases linearly at intermediate depth at 100°W in NEMO05 from 20°S to the equator, suggesting a slow isopycnal propagation (consistent with the experiments performed using NEMO2 in part 3.2). Conversely, the tracer accumulation is faster in the equatorial regions than in the mid-latitudes in NEMO01, suggesting a largeer role of advective transport, which is faster than the transport by isopycnal diffusive processes.

4.2.2 Equatorial IDW circulation origin thermocline water masslower 100°W, 5°N-5°S, 1000 m depth) is located in the larger intermediate eastern tropical pacific (IETP) ocean region (160°W – coast / 10°N-10°S / 200 – 2000 m). The particles originate close to the region of release (IETP) in 60 % of the cases in NEMO05 and 50 % of the cases in NEMO01, at a time scale of 50 years (Fig 7a and 8b). In NEMO05, after 50 years, the particles originating outside the IETP come either from the upper (0 – 200 m) ocean (5 %), deep (> 2000 m) ocean (1%),

higher (> 10°) latitudes (23 %), western (west of 160°W) part of the basin (21 %) (Fig 8d). The largest difference between NEMO05 and NEMO01 is the much larger amount of particles originating from the deep ocean in NEMO01 (8 % in NEMO01), suggesting the presence of vertical recirculation cells at intermediate depths. Despite the stronger EICS in NEMO01, the amount of particles originating from the western part of the basin is nearly identical in NEMO01 and NEMO05 after 50 years of integration. The advection processes are however faster in NEMO01, in particular the zonal advection. The relative difference between NEMO05 and NEMO1 is particularly strong 15 years after the release (approximately corresponding to the t10% at 1000 m at the equator in NEMO01), as already 10 % of the particles originate outside the IETP, in regions where the oxygen levels are high, in NEMO01 while this fraction is close to 0 in NEMO05.

The second release R2 (160°E, 5°N-5°S, 1000 m depth) is located in the intermediate western tropical pacific (IWTP) ocean region (160°W – coast / 10°N-10°S / 200 – 2000 m) (Fig 7b). After 50 years, all the particles originate outside of the IWTP in NEMO01 (Fig 8c) (50 % originate in the eastern basin, 23 % in the deep ocean, 24 % outside the equatorial band, 3 % in the upper 200 m) (Fig 8e) while only 70 % of the particles originate outside the IWTP in NEMO05 (39 % in the eastern basin, 27 % outside the equatorial band, 2 % in the deep ocean and 2 % in the upper ocean).

The Lagrangian experiments show a generally stronger ventilation at intermediate depth in NEMO01 due to the EICS, which reinforces the connections between western / eastern part of the basin and the thermocline / deep ocean.i Two releases R1 and R2 have been performed in the eastern and western part of the basin in order to assess the equatorial circulation in NEMO05 and NEMO01. A depth horizon of 1000 m has been chosen as it is a depth where the equatorial intermediate current system is relatively well developed in high resolution models and basically absent in coarse models (see Fig 5). Our results are not sensitive to the choice of another depth horizon in the range of 500 - 1500 m

The release R1 They also allow us to disentangle the transport of the resolved currents of the EICS (advection) from subgrid scale mixing processes, i.e. to assess the processes responsible for the equatorial ventilation.in the lower thermocline.Lagrangian particles (see 2.2.3) allow us to understand the origin of the waters

4.2.2 Equatorial IDW circulation

The analysis of the dispersion of Lagrangian particles (see 2.2.3) permits us to understand the origin of the waters circulating in the eastern part of the basin at IDW level. A total of 26515 particles have been released in the area located at 100°W, 10°N-10°S, 500-1500 m. These

particles have been integrated backward in time in order to determine their origin and the ventilation of the eastern tropical Pacific ocean (Fig 7).

After 5 years of backward integration we find that the particles originate from a well defined region, which extends from 110°W and 80°W to NEMO05 (Fig 7a). This region extends westward till 150°W, as a result of the stronger currents in NEMO01 (Fig 7b). This larger dispersion and westward origin of the particles is clearly visible after 10, 20 and 50 years of integration. In order to quantify the dispersion of the particles, we define the Intermediate Eastern Pacific Ocean (IETP) as the region 10°N-10°S, 500 – 1500 m, 160°W – coast. The particles originating outside of the IETP in close to 5 % / 50 % of the cases in NEMO05 and 10 % / 60 % of the cases of NEMO01, after a time scale of respectively 10 and 50 years. The Fig 7c shows a lag between NEMO01 and NEMO05 : while 10 % of the particles originate outside the IETP after 10 years in NEMO01 the same quantity is reached only after 20 years in NEMO05, suggesting a stronger transport in NEMO01. However, after the time period of 20 years, the number of particles originating outside the IETP does not grow faster any more in NEMO01 compared to NEMO05. A hypothesis is enhanced recirculation in NEMO01: the same particles may recirculate several times in the equatorial region due to alternating zonal jets in NEMO01.

The transport has been quantified based on this Lagrangian particles release (Fig 8). The volume transport is higher in NEMO01 (up to 0.2 Sv) (Fig 8a) compared to NEMO05 (less than 0.1 Sv at the equator) (Fig 8b). It also shows recirculating structures and alternating eastern and western transport in NEMO01 (Fig 8c). These recirculating structures are absent in NEMO05 and foster the dispersion of particles as shown above. The mean transport (zonal, meridional and vertical integration) in the region 10°N-10°S, 12E0°E-100°W is [value1] in NEMO01 and [value2] in NEMO05.

4.3 Model resolution and oxygen levels

The experiments discussed in 4.2 were not coupled with biogeochemical cycles for computational cost reasons. In order to assess the robustness of our findings (EICS plays a large role in setting tropical oxygen levels), we next analyze equatorial oxygen in a set of climate models similar to

547   CMIP models. To this end we use the GFDL model suite, characterized by a resolution increase
548   (GFDL1, GFDL025 and GFDL01 - see Table 1).

550   The striking difference between GFDL01 and GFDL025 / GFDL1 are the high oxygen levels in the
551   eastern part of the ocean below 1000 m in GFDL01 compared to GFDL025/GFDL1 (Fig 2). The
552   oxygen levels show weaker zonal gradient in GFDL01, consistent with the tracer experiment that
553   we performed in 4.2. and a more ventilated intermediate equatorial ocean. High values of mean
554   kinetic energy are associated with higher oxygen values (Fig 9). This is particularly clear in
555   GFDL01 at around 1500 m depth, where strong values of MKE are present and form the "bottom"
556   of the low oxygen volume (oxygen lower than 50 mmol.m-3). Conversely GFDL025 and GFDL1 do
557   not present high MKE values below 1000 m in the eastern part of the basin; the low oxygen volume
558   extends till depths greater than 2000 m. It suggests that intermediate currents participate in the
559   ventilation of the eastern tropical ocean and thus in limiting the vertical extension of the OMZ.

561   Oxygen levels do not increase linearly with the currents strength, i.e while currents strength
562   increase in GFDL1, GFDL025 and GFDL01, oxygen levels are relatively similar in GFDL1 and
563   GFDL025 (see Fig 5 and Fig 9). The relatively small net balance between large fluxes of
564   respiration and oxygen supply (Duteil et al., 2014) may be responsible for this behavior. If the
565   supply is slightly higher compared to the consumption by respiration, it will lead to an increase of
566   oxygen concentration. If it is slightly lower, the oxygen levels will decrease. A small difference in
567   supply (e.g slightly weaker currents) may therefore lead to a large difference in oxygen levels when
568   integrated over decades. For this reason, the impact of the EICS is more visible below 1000 m as
569   the respiration decreases following a power-law with depth (Martin et al., 1987) and is therefore
570   easier to offset even by a moderate oxygen supply.

572   Resolving explicitly the EICS results in a similar oxygen distribution to what Getzlaff and Dietze
573   (2013) (GD13) achieved with a simple EICS parameterization (Fig 9a): to compensate for the
574   "missing" EICS in UVIC, a coarse resolution model, they enhanced anisotropically the lateral
575   diffusivity in the equatorial region. The oxygen levels from UVIC GD13 are shown in blue contours
576   on top of the UVIC oxygen distribution (black) in Fig 9. Implementing this approach tends to
577   homogenize oxygen levels zonally, with an increase of the mean levels by 30-50 mmol.m^{-3} in the
578   eastern basin and a decrease of oxygen concentrations in the western basin. While this approach
579   may be useful to better represent the oxygen mean state, it however does not take in account the
580   potential variability and future evolution of the EICS.

582   **5. Summary and conclusions**

16   16

IDW are constituted by ~~Intermediate~~ waters masses ~~areDepth Waters (IDW)~~ which are subducted in the Southern Ocean and ~~-~~transported equatorward to the tropics by isopycnal processes (Sloyan and Kamenkovich, 2007; Sallee et al., 2013; Meijers, 2014) and the western boundary currents. At lower latitudes they recirculate into the lower thermocline of the tropical regions at 500 - 1500 m and into the EICS (Zenk et al., 2005; Marin et al., 2010; Cravatte et al., 2012; 2017; Ascani et al., 2015; Menesguen et al., 2019) (see schema Fig 1). We show here that the representation of this ventilation pathway is important to take into account when assessing tropical oxygen levels and the extent of the OMZ in coupled biogeochemical circulation or climate models. Particularly, we highlight two critical, yet typical, biases that hamper the correct representation of the tropical oxygen levels.

5.1 ~~Subducted~~ Subtropical IDW properties and tropical oxygen

First, the current generation of climate models, such as the CMIP5 models, show large deficiencies in simulating IDW. Along with an unrealistic representation of IDW ~~volume and~~ properties when the waters enter the subtropics, the models also lack the observed prominent oxygen maximum associated with IDW. Restoring oxygen levels to observed concentrations at 30°S/30°N and at 1500 m depth in a coarse resolution model, comparable to CMIP5 climate models in terms of resolution and oxygen bias, shows a significant impact on the lower thermocline (500 – 1500 m) oxygen levels: a positive anomaly of 60 $mmol.m^{-3}$ at midlatitudes translates into an oxygen increase by 10 $mmol-m^{-3}$ in tropical regions after 50 years of integration.

The equatorward transport of the anomaly in the subtropics is mostly due to isopycnal subgrid scale mixing processes as shown by the NEMO2 budget analysis. It suggests that mesoscale activity plays a major role in transporting IDW equatorward. In addition subsurface eddies may transport oxygen westward from the eastern Pacific ocean toward the mid-Pacific ocean region (Frenger et al., 2018, see their Fig 2).

5.2 ~~IMW transport and~~ Transport at IDW level and Equatorial Intermediate Current System

Second, the Equatorial Intermediate Current System (EICS) is not represented in coarse resolution models and only poorly represented in high resolution ocean circulation models (0.25° and 0.1°), as its strength remains too weak by a factor of two (consistent with previous studies, e.g Ascani et al., 2015). The EICS transports the IDW that occupies the lower thermocline (500 – 1500 m depth) and the recirculation of the IDW in the tropical ocean, as suggested by the observational study of Zenk et al. (2005), and shown in our study.

We investigated the impact of the EICS on the oxygen supply with tracer release experiments: the concentration of a conservative tracer that originates from the subtropical ocean, is, after 50 years,

620 30 % higher in the eastern equatorial (5°N-5S) Pacific in an ocean model with 0.1° resolution,
621 compared to an ocean model with 0.5 ° resolution. As the oxygen gradient along the equator is
622 similar to the gradient of the conservative tracer, we assume a similar enhancement of oxygen
623 supply by 30 % in the eastern equatorial Pacific at the same time scale. This means, if we account
624 for oxygen consumption due to respiration (about 1 $mmol.m^{-3}.yr^{-1}$ between 5°N-5°S, see section
625 3.2), that the better resolved EICS in the higher resolution ocean leads roughly to higher
626 intermediate oxygen levels of 15 - 30 $mmol-m^{-3}$ compared to the lower resolution ocean experiment
627 in a timescale of 50 years. Consistently, the 0.1°-ocean GFDL01 model displays oxygen
628 concentrations larger by about 30 $mmol.m^{-3}$ in the eastern equatorial lower thermocline (500-1500
629 m) compared to the 1°-ocean GFDL1 configuration (with higher subtropical oxygen concentrations
630 of IWM of 15 $mmol.m^{-3}$ in GFDL01 at 30°S)

631

632 We would like to highlight two potential implications of our finding of the important role of the EICS
633 for the Pacific eastern tropical oxygen supply: i) First, we have shown that the intermediate current
634 system EICS is important for the connection between the western and eastern Pacific Ocean at a
635 decadal / multidecadal time scale. This suggests that the EICS modulates the mean state and the
636 variability of the tropical oxygen in the lower thermocline, and subsequently the whole water
637 column by upwelling of deep waters. ii) Second, we have found an enhancement of the
638 connections between the equatorial deep ocean (> 2000 m) and the lower thermocline if the
639 resolution of a model is enhanced. This result is consistent with the studies of Brandt et al. (2011,
640 2012), who suggested, based on observational data and on an idealized model, that Equatorial
641 Deep Jets as part of the EICS (see Fig 1b) propagate their energy upward and impact the upper
642 ocean properties of the ocean, including their oxygen content. Taken this into account, we
643 hypothesize that the Pacific Deep Water has a larger role than previously thought in modulating the
644 intermediate and upper ocean properties.

645

646 A pragmatic approach to account for the missing EICS is to increase diffusion anisotropically, with
647 increased zonal mixing in the tropics (Getzlaff and Dietze, 2013). This parameterization mimics a
648 more vigorous EICS and improves the simulated shape of the OMZ in climate models. However,
649 the prominent bias of IDW in climate models, and therefore of the water masses entering the EICS
650 is not accounted for with this parameterization. Furthermore such a parameterization improves the
651 mean state but does not reproduce the variability of the EICS.

652

653 5.3 Implication for biogeochemical cycles
654 The IDW are an important important supplier of oxygen to the tropical oceans, but also of nutrients
655 (Palter et al., 2010) as well as anthropogenic carbon (e.g Kathiwala et al., 2012), which
656 accumulates in mode and intermediate waters of the Southern Ocean (Sabine et al., 2004;

657 Resplandy et al., 2013). The mechanisms that we discussed here may therefore play a role in
658 ocean carbon climate feedbacks on time scales of decades to a century.

659

660 This study shows that there is a need to look with greater care into IDW properties to understand
661 the tropical oxygen distribution in models, in particular in CMIP class models. As shown by
662 Kwiatkowski et al. (2020), CMIP6 models (typical horizontal resolution of 1°) do not agree on the
663 future change in tropical oxygen levels (mean 100 – 600m, their Fig 2). This may partly originate in
664 a misrepresentation of the properties of the IDW in the different models and the strength of the
665 connection between western and eastern Pacific Ocean. Simple analyses, similar to our Fig 2
666 (oxygen levels at 30°S and oxygen levels in the eastern tropical Pacific) and Fig 9 (Mean Kinetic
667 Energy at intermediate depth) may give some insight into the mechanisms at play. In addition,
668 analyses of experiments performed in the context of the High Resolution Model Intercomparison
669 Project (resolution greater than 0.25°) (Haarsma et al., 2016), part of CMIP6, will give a more
670 complete insight on whether a significant Equatorial Intermediate Current System develops at
671 higher resolution. While HighResMIP are not coupled with a biogeochemical module, velocity fields
672 are available at a monthly resolution, which allows to perform "offline" tracer or Lagrangian particle
673 experiments.

674

675 Finally, this study suggests that changes of the properties of the IDW may contribute to the still
676 partly unexplained deoxygenation of 5 mmol.m^{-3} / decade occurring in the lower thermocline of the
677 equatorial eastern Pacific Ocean (Schmidtko et al., 2017; Oschlies et al., 2018). In addition to an
678 oxygen decrease in tropical regions, Schmidtko et al. (2017) showed a decrease of oxygen levels
679 by 2-5 mmol.m^{-3} in the regions of formations of AAIW. Based on repeated cruise observations,
680 Panassa et al. (2018) highlighted an increase of the apparent oxygen utilization in the core of the
681 AAIW, together with a 5 % increase in nutrient concentrations from 1990 to 2014. The transport of
682 this modified AAIW, poorer in oxygen and richer in nutrients, toward the low latitudes both by small
683 scale processes (section 3) and at the equator by the EICS (section 4), may explain a significant
684 part of the occurring deoxygenation in the equatorial ocean. In addition to changes in the AAIW
685 properties, little is known about the variability and long term trend of the strength of the EICS, an
686 oceanic "bridge" between the western and the eastern part of the basin. After our first steps toward
687 assessing the role of extratropical oxygen characteristics and the zonal transport of waters at
688 intermediate depths for tropical oxygen concentration, a possible way forward to further assess this
689 cascade of biases could be to perform idealized model experiments in high resolution
690 configurations, aiming to assess both the effect of the observed change in the AAIW properties and
691 of a potential change of EICS strength on oxygen levels.

692

693

Data and code availability

The code for the Nucleus for European Modeling of the Ocean (NEMO) is available at: https://www.nemo-ocean.eu/. The code for the University of Victoria (UVIC) model is available at :http://terra.seos.uvic.ca/model/. The Lagrangian particles ARIANE code is available at http://stockage.univ-brest.fr/~grima/Ariane/. The Coordinated Ocean-ice Reference Experiments (COREv2) dataset is available at: https://data1.gfdl.noaa.gov/nomads/forms/core/COREv2.html. The experiments data is available on request.

Authors contributions

OD conceived the study, performed the NEMO model and ARIANE experiments and analyzed the data. IF preprocessed and helped to analyze the GFDL data. JG preprocessed and helped to analyze the UVIC data. All authors discussed the results and wrote the manuscript.

Competing interest

The authors declare that they have no conflict of interest.

Acknowledgments

This work is a contribution of the SFB754 "Climate-Biogeochemistry Interactions in the Tropical Ocean", supported by the Deutsche Forschungsgemeinschaft (DFG). The NEMO simulations were performed at the North German Supercomputing Alliance (HLRN). We would like to thank Markus Scheinert (research unit "Ocean Dynamics", GEOMAR) for his technical support in compiling the NEMO code and for providing the high resolution NEMO input files. We would like to thank GFDL for producing the CM2-0 suite that involved a substantial commitment of computational resources and data storage. J.G acknowledges support by the project "Reduced Complexity Models" (supported by the Helmholtz Association of German Research Centres (HGF) – grant no. ZT-I-0010). I.F. acknowledges the German Federal Ministry of Education and Research (BMBF) project CUSCO (grant no. 03F0813A). O.D acknowledges the German Research Foundation (DFG) (grant no. 434479332)

References

Ascani, F., Firing, E., Dutrieux, P., McCreary, J. P., & Ishida, A. (2010). Deep Equatorial Ocean Circulation Induced by a Forced–Dissipated Yanai Beam. Journal of Physical Oceanography, 40(5), 1118–1142. doi:10.1175/2010jpo4356.1

Ascani, F., Firing, E., McCreary, J. P., Brandt, P., & Greatbatch, R. J. (2015). The Deep Equatorial Ocean Circulation in Wind-Forced Numerical Solutions. Journal of Physical Oceanography, 45(6), 1709–1734. doi:10.1175/jpo-d-14-0171.1

Bahl, A., Gnanadesikan, A., & Pradal, M. A. (2019). Variations in Ocean Deoxygenation Across Earth System Models: Isolating the Role of Parameterized Lateral Mixing. Global Biogeochemical Cycles, 33(6), 703–724. doi:10.1029/2018gb006121

Blanke, B., & Raynaud, S. (1997). Kinematics of the Pacific Equatorial Undercurrent: An Eulerian and Lagrangian Approach from GCM Results. Journal of Physical Oceanography, 27(6), 1038–1053. doi:10.1175/1520-0485(1997)027<1038:kotpeu>2.0.co;2

Brandt, P., Funk, A., Hormann, V., Dengler, M., Greatbatch, R. J., & Toole, J. M. (2011). Interannual atmospheric variability forced by the deep equatorial Atlantic Ocean. Nature, 473(7348), 497–500. doi:10.1038/nature10013

Brandt, P., Greatbatch, R. J., Claus, M., Didwischus, S.-H., Hormann, V., Funk, A., … Körtzinger, A. (2012). Ventilation of the equatorial Atlantic by the equatorial deep jets. Journal of Geophysical Research: Oceans, 117(C12), n/a–n/a. doi:10.1029/2012jc008118

Breitburg, D., Levin, L. A., Oschlies, A., Grégoire, M., Chavez, F. P., Conley, D. J., … Zhang, J. (2018). Declining oxygen in the global ocean and coastal waters. Science, 359(6371), eaam7240. doi:10.1126/science.aam7240

Busecke, J. J. M., Resplandy, L., & Dunne, J. P. (2019). The Equatorial Undercurrent and the Oxygen Minimum Zone in the Pacific. Geophysical Research Letters, 46(12), 6716–6725. doi:10.1029/2019gl082692

Cabré, A., Marinov, I., Bernardello, R., & Bianchi, D. (2015). Oxygen minimum zones in the tropical Pacific across CMIP5 models: mean state differences and climate change trends. Biogeosciences, 12(18), 5429–5454. doi:10.5194/bg-12-5429-2015

Carrasco, C., Karstensen, J., & Farias, L. (2017). On the Nitrous Oxide Accumulation in Intermediate Waters of the Eastern South Pacific Ocean. Frontiers in Marine Science, 4. doi:10.3389/fmars.2017.00024

Cravatte, S., Kessler, W. S., & Marin, F. (2012). Intermediate Zonal Jets in the Tropical Pacific Ocean Observed by Argo Floats. Journal of Physical Oceanography, 42(9), 1475–1485. doi:10.1175/jpo-d-11-0206.1

Cravatte, S., Kestenare, E., Marin, F., Dutrieux, P., & Firing, E. (2017). Subthermocline and Intermediate Zonal Currents in the Tropical Pacific Ocean: Paths and Vertical Structure. Journal of Physical Oceanography, 47(9), 2305–2324. doi:10.1175/jpo-d-17-0043.1

Czeschel, R., Stramma, L., Schwarzkopf, F. U., Giese, B. S., Funk, A., and Karstensen, J. (2011), Middepth circulation of the eastern tropical South Pacific and its link to the oxygen minimum zone, J. Geophys. Res., 116, C01015, doi:10.1029/2010JC006565

Delworth, T. L., Rosati, A., Anderson, W., Adcroft, A. J., Balaji, V., Benson, R., … Zhang, R. (2012). Simulated Climate and Climate Change in the GFDL CM2.5 High-Resolution Coupled Climate Model. Journal of Climate, 25(8), 2755–2781. doi:10.1175/jcli-d-11-00316.1

Dietze, H., & Loeptien, U. (2013). Revisiting "nutrient trapping" in global coupled biogeochemical ocean circulation models. Global Biogeochemical Cycles, 27(2), 265–284. doi:10.1002/gbc.20029

Dufour, C. O., Griffies, S. M., de Souza, G. F., Frenger, I., Morrison, A. K., Palter, J. B., … Slater, R. D. (2015). Role of Mesoscale Eddies in Cross-Frontal Transport of Heat and Biogeochemical Tracers in the Southern Ocean. Journal of Physical Oceanography, 45(12), 3057–3081. doi:10.1175/jpo-d-14-0240.1

Duteil, O., & Oschlies, A. (2011). Sensitivity of simulated extent and future evolution of marine suboxia to mixing intensity. Geophysical Research Letters, 38(6), n/a–n/a. doi:10.1029/2011gl046877

Duteil, O., Koeve, W., Oschlies, A., Aumont, O., Bianchi, D., Bopp, L., … Segschneider, J. (2012). Preformed and regenerated phosphate in ocean general circulation models: can right total concentrations be wrong? Biogeosciences, 9(5), 1797–1807. doi:10.5194/bg-9-1797-2012

Duteil, O., Böning, C. W., & Oschlies, A. (2014). Variability in subtropical-tropical cells drives oxygen levels in the tropical Pacific Ocean. Geophysical Research Letters, 41(24), 8926–8934. doi:10.1002/2014gl061774

Duteil, O., Oschlies, A., & Böning, C. W. (2018). Pacific Decadal Oscillation and recent oxygen decline in the eastern tropical Pacific Ocean. Biogeosciences, 15(23), 7111–7126. doi:10.5194/bg-15-7111-2018

Duteil, O. (2019). Wind Synoptic Activity Increases Oxygen Levels in the Tropical Pacific Ocean. Geophysical Research Letters, 46(5), 2715–2725. doi:10.1029/2018gl081041

Eden, C., & Dengler, M. (2008). Stacked jets in the deep equatorial Atlantic Ocean. Journal of Geophysical Research, 113(C4). doi:10.1029/2007jc004298

Emery, W. J. 2003. Water types and water masses. In: Encyclopedia of Atmospheric Sciences. 2nd ed. (eds. J.R. Holton, J.A. Curry and J.A. Pyle). Elsevier, Atlanta, GA, pp. 1556–1567

Firing, E., Wijffels, S. E., & Hacker, P. (1998). Equatorial subthermocline currents across the Pacific. Journal of Geophysical Research: Oceans, 103(C10), 21413–21423. doi:10.1029/98jc01944

Firing, E. (1987). Deep zonal currents in the central equatorial Pacific. Journal of Marine Research, 45(4), 791–812. doi:10.1357/002224087788327163

Frenger, I., Bianchi, D., Stührenberg, C., Oschlies, A., Dunne, J., Deutsch, C., … Schütte, F. (2018). Biogeochemical Role of Subsurface Coherent Eddies in the Ocean: Tracer Cannonballs, Hypoxic Storms, and Microbial Stewpots? Global Biogeochemical Cycles, 32(2), 226–249. doi:10.1002/2017gb005743

Galbraith, E. D., Dunne, J. P., Gnanadesikan, A., Slater, R. D., Sarmiento, J. L., Dufour, C. O., … Marvasti, S. S. (2015). Complex functionality with minimal computation: Promise and pitfalls of reduced-tracer ocean biogeochemistry models. Journal of Advances in Modeling Earth Systems, 7(4), 2012–2028. doi:10.1002/2015ms000463

803 Garcia, H. E., K. Weathers, C. R. Paver, I. Smolyar, T. P. Boyer, R. A. Locarnini, M. M. Zweng, A.
804 V. Mishonov, O. K. Baranova, D. Seidov, and J. R. Reagan, 2018. *World Ocean Atlas 2018,*
805 *Volume 3: Dissolved Oxygen, Apparent Oxygen Utilization, and Oxygen Saturation*. A. Mishonov
806 Technical Ed.; NOAA Atlas NESDIS 83, 38pp.

807 Getzlaff, J., & Dietze, H. (2013). Effects of increased isopycnal diffusivity mimicking the unresolved
808 equatorial intermediate current system in an earth system climate model. Geophysical Research
809 Letters, 40(10), 2166–2170. doi:10.1002/grl.50419

810 Gnanadesikan, A., Bianchi, D., & Pradal, M. (2013). Critical role for mesoscale eddy diffusion in
811 supplying oxygen to hypoxic ocean waters. Geophysical Research Letters, 40(19), 5194–5198.
812 doi:10.1002/grl.50998

813 Gouriou, Y., Delcroix, T., & Eldin, G. (2006). Upper and intermediate circulation in the western
814 equatorial Pacific Ocean in October 1999 and April 2000. Geophysical Research Letters, 33(10), n/
815 a–n/a. doi:10.1029/2006gl025941

816 Griffies, S. M., Winton, M., Anderson, W. G., Benson, R., Delworth, T. L., Dufour, C. O., … Zhang,
817 R. (2015). Impacts on Ocean Heat from Transient Mesoscale Eddies in a Hierarchy of Climate
818 Models. Journal of Climate, 28(3), 952–977. doi:10.1175/jcli-d-14-00353.1

819 Haarsma, R. J., Roberts, M. J., Vidale, P. L., Senior, C. A., Bellucci, A., Bao, Q., Chang, P., Corti,
820 S., Fučkar, N. S., Guemas, V., von Hardenberg, J., Hazeleger, W., Kodama, C., Koenigk, T.,
821 Leung, L. R., Lu, J., Luo, J.-J., Mao, J., Mizielinski, M. S., Mizuta, R., Nobre, P., Satoh, M.,
822 Scoccimarro, E., Semmler, T., Small, J., and von Storch, J.-S.(2016). High Resolution Model
823 Intercomparison Project (HighResMIPv1.0)forCMIP6, Geosci. Model Dev., 9, 4185–4208,
824 https://doi.org/10.5194/gmd-9-4185-2016

825 Iudicone, D., Rodgers, K. B., Schopp, R., & Madec, G. (2007). An Exchange Window for the
826 Injection of Antarctic Intermediate Water into the South Pacific. Journal of Physical Oceanography,
827 37(1), 31–49. doi:10.1175/jpo2985.1

828 Izumo, T. (2005). The equatorial undercurrent, meridional overturning circulation, and their roles in
829 mass and heat exchanges during El Niño events in the tropical Pacific ocean. Ocean Dynamics,
830 55(2), 110–123. doi:10.1007/s10236-005-0115-1

831 Khatiwala, S., Tanhua, T., Mikaloff Fletcher, S., Gerber, M., Doney, S. C., Graven, H. D., …
832 Sabine, C. L. (2013). Global ocean storage of anthropogenic carbon. Biogeosciences, 10(4),
833 2169–2191. doi:10.5194/bg-10-2169-2013

834 Kawabe, M., , Y. Kashino, , and Y. Kuroda, (2008): Variability and linkages of New Guinea coastal
835 undercurrent and lower equatorial intermediate current. *J. Phys. Oceanogr.*, 38, 1780–1793,
836 doi:10.1175/2008JPO3916.1.

837 Kawabe, M., & Fujio, S. (2010). Pacific ocean circulation based on observation. Journal of
838 Oceanography, 66(3), 389–403. doi:10.1007/s10872-010-0034-8

839 Keller, D. P., Oschlies, A., & Eby, M. (2012). A new marine ecosystem model for the University of
840 Victoria Earth System Climate Model. Geoscientific Model Development, 5(5), 1195–1220.
841 doi:10.5194/gmd-5-1195-2012

842 Koshlyakov, M.N. and Tarakanov, R.Y. (2003). Antarctic Bottom Water in the Pacific sector of the
843 Southern Ocean, Oceanology 43(1):1-15

844 Kriest, I., Khatiwala, S., & Oschlies, A. (2010). Towards an assessment of simple global marine
845 biogeochemical models of different complexity. Progress in Oceanography, 86(3-4), 337–360.
846 doi:10.1016/j.pocean.2010.05.002

847 Kwiatkowski, L., Torres, O., Bopp, L., Aumont, O., Chamberlain, M., Christian, J. R., Dunne, J. P.,
848 Gehlen, M., Ilyina, T., John, J. G., Lenton, A., Li, H., Lovenduski, N. S., Orr, J. C., Palmieri, J.,
849 Santana-Falcón, Y., Schwinger, J., Séférian, R., Stock, C. A., Tagliabue, A., Takano, Y., Tjiputra,
850 J., Toyama, K., Tsujino, H., Watanabe, M., Yamamoto, A., Yool, A., and Ziehn, T.: Twenty-first
851 century ocean warming, acidification, deoxygenation, and upper-ocean nutrient and primary
852 production decline from CMIP6 model projections, Biogeosciences, 17, 3439–3470, https://doi.org/
853 10.5194/bg-17-3439-2020, 2020.

854 Lachkar, Z., Orr, J. C., & Dutay, J.-C. (2009). Seasonal and mesoscale variability of oceanic
855 transport of anthropogenic CO2. Biogeosciences, 6(11), 2509–2523. doi:10.5194/bg-6-2509-2009

856 Large, W. G., & Yeager, S. G. (2008). The global climatology of an interannually varying air–sea
857 flux data set. Climate Dynamics, 33(2-3), 341–364. doi:10.1007/s00382-008-0441-3

858 Locarnini, R.A., T.P. Boyer, A.V. Mishonov, J.R. Reagan, M.M. Zweng, O.K. Baranova, H.E.
859 Garcia, D. Seidov, K.W. Weathers, C.R. Paver, and I.V. Smolyar (2019). World Ocean Atlas 2018,
860 Volume 5: Density. A. Mishonov, Technical Editor. NOAA Atlas NESDIS 85, 41pp.

861 Lübbecke, J. F., Böning, C. W., & Biastoch, A. (2008). Variability in the subtropical-tropical cells
862 and its effect on near-surface temperature of the equatorial Pacific: a model study. Ocean Science,
863 4(1), 73–88. doi:10.5194/os-4-73-2008

864 Madec, G.., Bourdallé-Badie, R., Pierre-Antoine Bouttier, Bricaud, C., Bruciaferri, D., Calvert, D.,
865 Chanut, J., Clementi, E., Coward, A., Delrosso, D., Ethé, C., Flavoni, S., Graham, T., Harle, J.,
866 Iovino, D., Lea, D., Lévy, C., Lovato, T., Martin, N., … Vancoppenolle, M. (2017). NEMO ocean
867 engine. https://doi.org/10.5281/ZENODO.3248739Marin, F., Kestenare, E., Delcroix, T., Durand,
868 F., Cravatte, S., Eldin, G., & Bourdallé-Badie, R. (2010). Annual Reversal of the Equatorial
869 Intermediate Current in the Pacific: Observations and Model Diagnostics. Journal of Physical
870 Oceanography, 40(5), 915–933. doi:10.1175/2009jpo4318.1

871 Martin, J. H., Knauer, G. A., Karl, D. M., & Broenkow, W. W. (1987). VERTEX: carbon cycling in
872 the northeast Pacific. Deep Sea Research Part A. Oceanographic Research Papers, 34(2), 267–
873 285. doi:10.1016/0198-0149(87)90086-0

874 Meijers, A. J. S. (2014). The Southern Ocean in the Coupled Model Intercomparison Project phase
875 5. Philosophical Transactions of the Royal Society A: Mathematical, Physical and Engineering
876 Sciences, 372(2019), 20130296. doi:10.1098/rsta.2013.0296

877 Ménesguen, C., Delpech, A., Marin, F., Cravatte, S., Schopp, R., & Morel, Y. (2019). Observations
878 and Mechanisms for the Formation of Deep Equatorial and Tropical Circulation. Earth and Space
879 Science, 6(3), 370–386. doi:10.1029/2018ea000438

880 Molinelli EJ (1981) The Antarctic influence on Antarctic Intermediate Water. J Mar Res 39:267–293

881 Oschlies, A., Brandt, P., Stramma, L., & Schmidtko, S. (2018). Drivers and mechanisms of ocean
882 deoxygenation. Nature Geoscience, 11(7), 467–473. doi:10.1038/s41561-018-0152-2

883 Palter, J. B., Sarmiento, J. L., Gnanadesikan, A., Simeon, J., and Slater, R. D. (2010). Fueling
884 export production: nutrient return pathways from the deep ocean and their dependence on the
885 Meridional Overturning Circulation, Biogeosciences, 7, 3549–3568, doi:10.5194/bg-7-3549-2010

886 Panassa, E., Santana-Casiano, J. M., González-Dávila, M., Hoppema, M., van Heuven, S. M. A. .,
887 Völker, C., … Hauck, J. (2018). Variability of nutrients and carbon dioxide in the Antarctic
888 Intermediate Water between 1990 and 2014. Ocean Dynamics, 68(3), 295–308.
889 doi:10.1007/s10236-018-1131-2

890 Pardo, P. C., Pérez, F. F., Velo, A., & Gilcoto, M. (2012). Water masses distribution in the
891 Southern Ocean: Improvement of an extended OMP (eOMP) analysis. Progress in Oceanography,
892 103, 92–105. doi:10.1016/j.pocean.2012.06.002

893 Paulmier, A., Ruiz-Pino (2009), D. Oxygen minimum zones (OMZs) in the modern ocean,Progress
894 in Oceanography, 80(3), 113-128, doi:10.1016/j.pocean.2008.08.001.

895 Qu, T., & Lindstrom, E. J. (2004). Northward Intrusion of Antarctic Intermediate Water in the
896 Western Pacific*. Journal of Physical Oceanography, 34(9), 2104–2118. doi:10.1175/1520-
897 0485(2004)034<2104:nioaiw>2.0.co;2

898 Resplandy, L., Bopp, L., Orr, J. C., & Dunne, J. P. (2013). Role of mode and intermediate waters in
899 future ocean acidification: Analysis of CMIP5 models. Geophysical Research Letters, 40(12),
900 3091–3095. doi:10.1002/grl.50414

901 Rowe, G. D., Firing, E., & Johnson, G. C. (2000). Pacific Equatorial Subsurface Countercurrent
902 Velocity, Transport, and Potential Vorticity*. Journal of Physical Oceanography, 30(6), 1172–1187.
903 doi:10.1175/1520-0485(2000)030<1172:pescvt>2.0.co;2

904 Russell, J. L., & Dickson, A. G. (2003). Variability in oxygen and nutrients in South Pacific Antarctic
905 Intermediate Water. Global Biogeochemical Cycles, 17(2), n/a–n/a. doi:10.1029/2000gb001317

906 Sabine, C. L. (2004). The Oceanic Sink for Anthropogenic CO2. Science, 305(5682), 367–371.
907 doi:10.1126/science.1097403

908 Sallée, J.-B., Shuckburgh, E., Bruneau, N., Meijers, A. J. S., Bracegirdle, T. J., Wang, Z., & Roy, T.
909 (2013). Assessment of Southern Ocean water mass circulation and characteristics in CMIP5

910   models: Historical bias and forcing response. Journal of Geophysical Research: Oceans, 118(4),

911   1830–1844. doi:10.1002/jgrc.20135

912   Schmidtko, S., Stramma, L., & Visbeck, M. (2017). Decline in global oceanic oxygen content during

913   the past five decades. Nature, 542(7641), 335–339. doi:10.1038/nature21399

914   Sen Gupta, A., & England, M. H. (2007). Evaluation of Interior Circulation in a High-Resolution

915   Global Ocean Model. Part II: Southern Hemisphere Intermediate, Mode, and Thermocline Waters.

916   Journal of Physical Oceanography, 37(11), 2612–2636. doi:10.1175/2007jpo3644.1

917   Shigemitsu, M., Yamamoto, A., Oka, A., & Yamanaka, Y. (2017). One possible uncertainty in

918   CMIP5 projections of low-oxygen water volume in the Eastern Tropical Pacific. Global

919   Biogeochemical Cycles, 31(5), 804–820. doi:10.1002/2016gb005447

920   Sloyan, B. M., & Kamenkovich, I. V. (2007). Simulation of Subantarctic Mode and Antarctic

921   Intermediate Waters in Climate Models. Journal of Climate, 20(20), 5061–5080.

922   doi:10.1175/jcli4295.1

923   Sloyan, B. M., & Rintoul, S. R. (2001). Circulation, Renewal, and Modification of Antarctic Mode

924   and Intermediate Water*. Journal of Physical Oceanography, 31(4), 1005–1030. doi:10.1175/1520-

925   0485(2001)031<1005:cramoa>2.0.co;2

926   Takano, Y., Ito, T., & Deutsch, C. (2018). Projected Centennial Oxygen Trends and Their

927   Attribution to Distinct Ocean Climate Forcings. Global Biogeochemical Cycles, 32(9), 1329–1349.

928   doi:10.1029/2018gb005939

929   Talley, L. D. (1993). Distribution and Formation of North Pacific Intermediate Water. Journal of

930   Physical Oceanography, 23(3), 517–537. doi:10.1175/1520-0485(1993)023<0517:dafonp>2.0.co;2

931   Weaver, A. J., Eby, M., Wiebe, E. C., Bitz, C. M., Duffy, P. B., Ewen, T. L., … Yoshimori, M.

932   (2001). The UVic earth system climate model: Model description, climatology, and applications to

933   past, present and future climates. Atmosphere-Ocean, 39(4), 361–428.

934   doi:10.1080/07055900.2001.9649686

935   Xu, L., Li, P., Xie, S. et al. (2016). Observing mesoscale eddy effects on mode-water subduction

936   and transport in the North Pacific. Nature Communications, 10505 (2016),

937   doi.org/10.1038/ncomms10505

938   Zenk, W., Siedler, G., Ishida, A., Holfort, J., Kashino, Y., Kuroda, Y., … Müller, T. J. (2005).

939   Pathways and variability of the Antarctic Intermediate Water in the western equatorial Pacific

940   Ocean. Progress in Oceanography, 67(1-2), 245–281. doi:10.1016/j.pocean.2005.05.003

941   Zhu, C., Liu, Z., & Gu, S. (2017). Model bias for South Atlantic Antarctic intermediate water in

942   CMIP5. Climate Dynamics, 50(9-10), 3613–3624. doi:10.1007/s00382-017-3828-1

943

944

945

946

947

948

949

950

951

952

953

954

955

956

957

958

959

960

961

962

963

964

965

966

967

968

969

970

971

972

973

974

975

976

977

978

979

980

981

982

983

984

985

986

987

Figures and Table

989
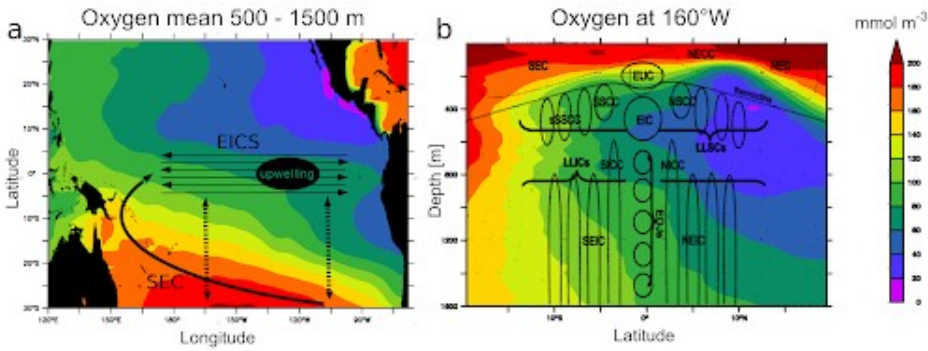
991 **[Figure above is replaced by Fig below]**

992

993

994

995
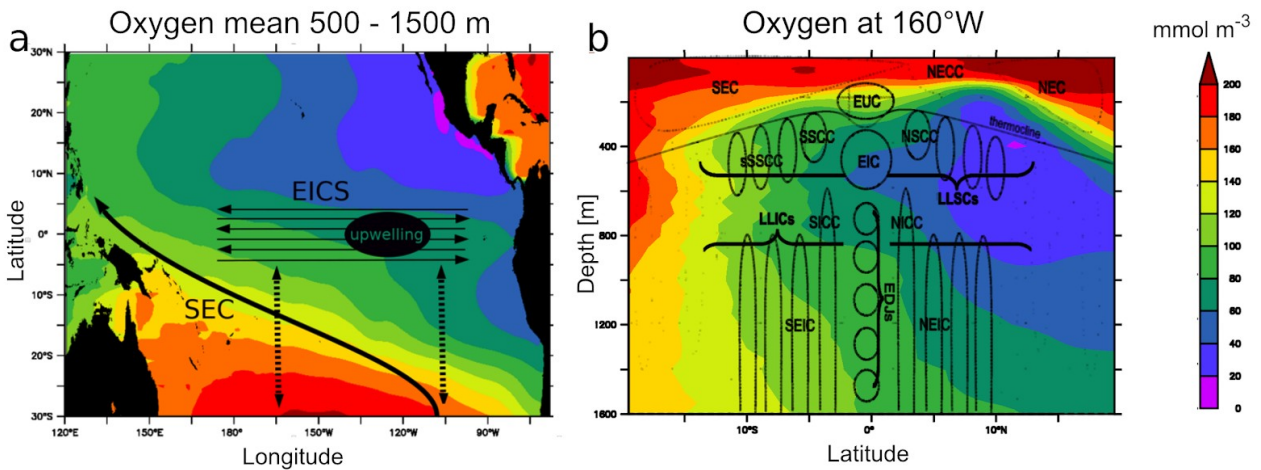
Figure 1 : a- schema summarizing the intermediate water masses (IWM) pathway from the subtropics into the equatorial regions. EICS : Equatorial Intermediate Current System. SEC : South Equatorial Current (Kawabe et al., 2008). Dashed line : isopycnal diffusive processes. Observed (World Ocean Atlas) oxygen levels (mmol.m^{-3}) in the lower thermocline (mean 500-1500m) are represented in color. b - schema (adapted from Menesguen et al., 2019) illustrating the complexity of the EICS, extending below the thermocline till more than 2000 m depth (see section 4.1 for a detailed description). Observed (World Ocean Atlas) oxygen levels at 160°W are represented in color. SEC : South Equatorial Current. N/SEC : North/South Equatorial Current. NECC: North Equatorial Counter Current. EUC : Equatorial Undercurrent. EIC : Equatorial Intermediate Current. N/SSCC : North / South Subsurface Counter Current. LLSC : Low Latitude Subsurface Currents.

1006   LLIC : Low Latitudes Intermediate Currents. N/SEIC : North / South Equatorial Intermediate
1007   Current. N/SICC : North / South Intermediate Current. EDJ : Equatorial Deep Jets.
1008
1009
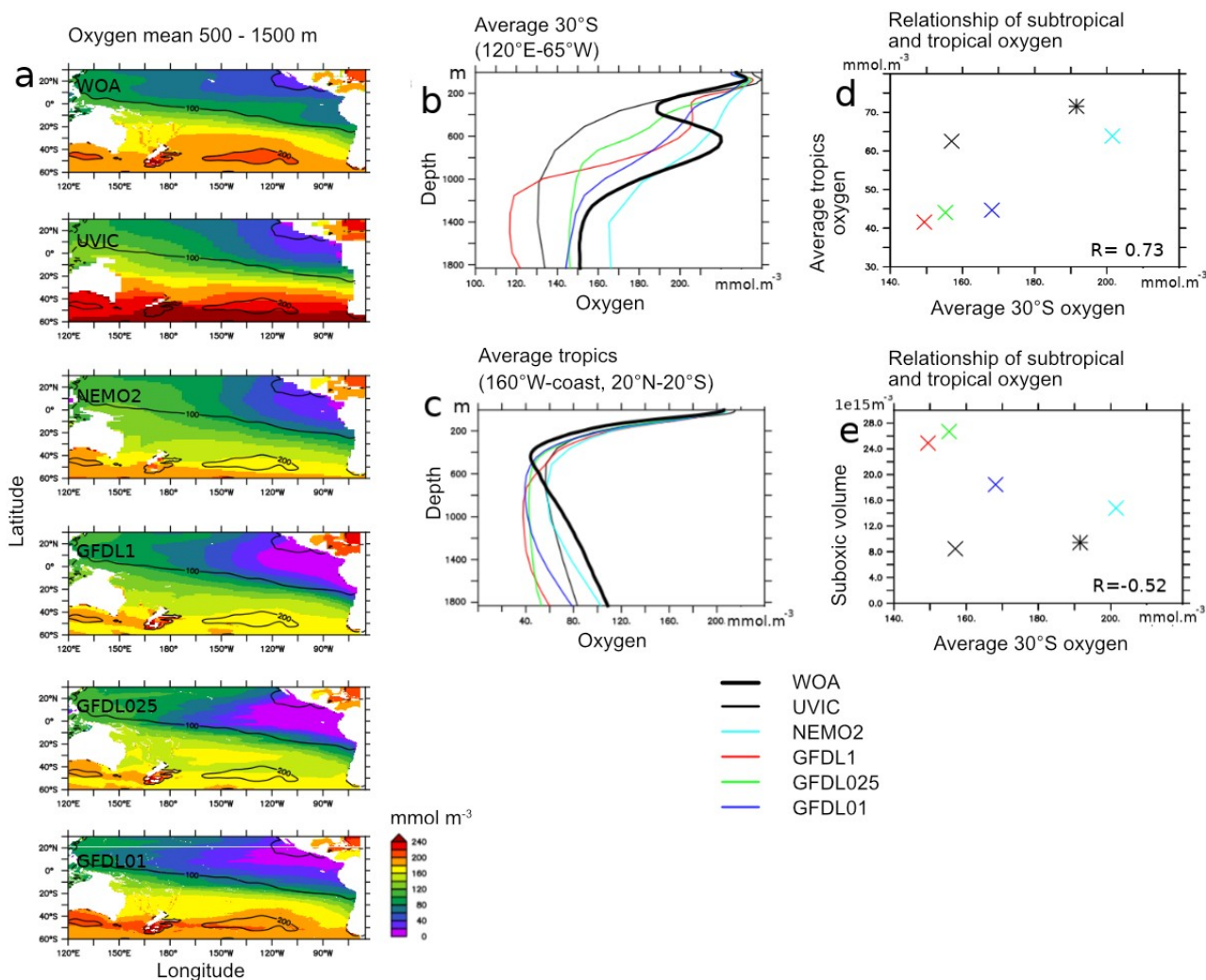
1010
1011
1012
1013
1014
1015
1016
1017   Figure 2 : a- oxygen levels (mmol.m^{-3}) in observations (World Ocean Atlas - WOA) (mean 500 –
1018   1500 m) and models (UVIC, NEMO2, GFDL1, GFDL025, GFDL01). Contours correspond to WOA
1019   values. b: average "30°S" (120°E-65°W, 30°S) c : average "tropics" (160°W-coast, 20°N-20°S). d:
1020   average "30°S" vs "tropics". e: average "30°S" vs volume of tropical suboxic ocean (oxygen lower
1021   than 20 mmol.m^{-3}) regions (1e15m3). b-e : UVIC : black, NEMO2 : cyan, GFDL1 : red, GFDL025,
1022   green; GFDL01 : blue, WOA: bold line (b,c) and star (d,e).
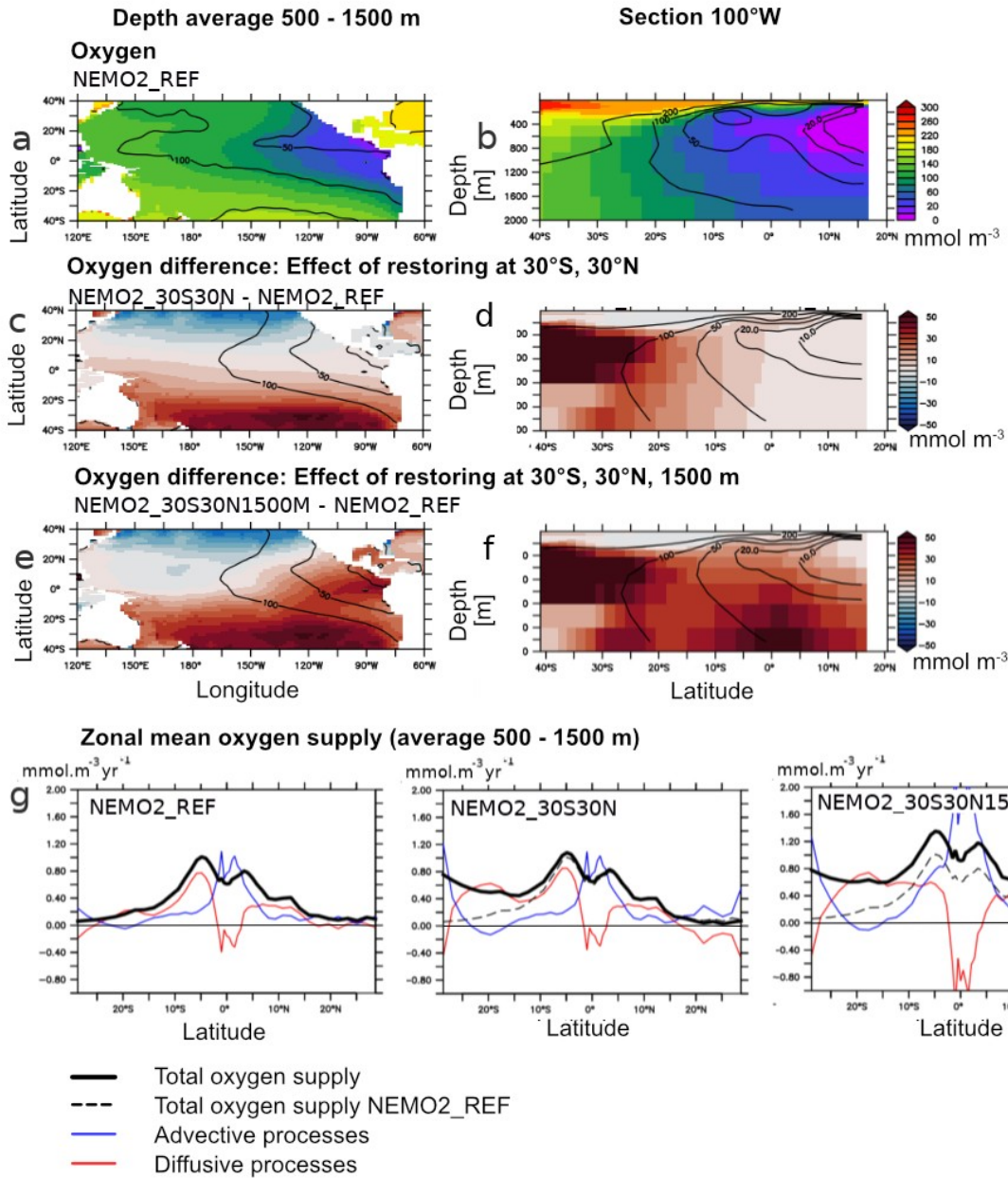
1024 Figure 3 : a,b: Oxygen (mmol.m^{-3}) in the experiments NEMO2_REF (color) and World Ocean Atlas
1025 (contour) (a- average 500-1500 m, b- 100°W). c,d: Oxygen (mmol.m^{-3}) difference (c- average 500 –
1026 1500m, d- 100°W) between the experiments NEMO2_30S30N minus NEMO2_REF. e,f : Oxygen
1027 (mmol.m^{-3}) difference (e- average 500-1500m, f- 100°W) between the experiments
1028 NEMO2_30S30N1500M minus NEMO2_REF. g- basin zonal average (average 500 - 1500 m) of
1029 the oxygen total supply (bold) (mmol.m^{-3}.year^{-1}), advective processes (blue) and isopycnal diffusion
1030 (red) in NEMO2_REF, NEMO2_30S30N, NEMO2_30S30N1500M. The dashed line is the oxygen
1031 total supply in NEMO2_REF.

1032

1033
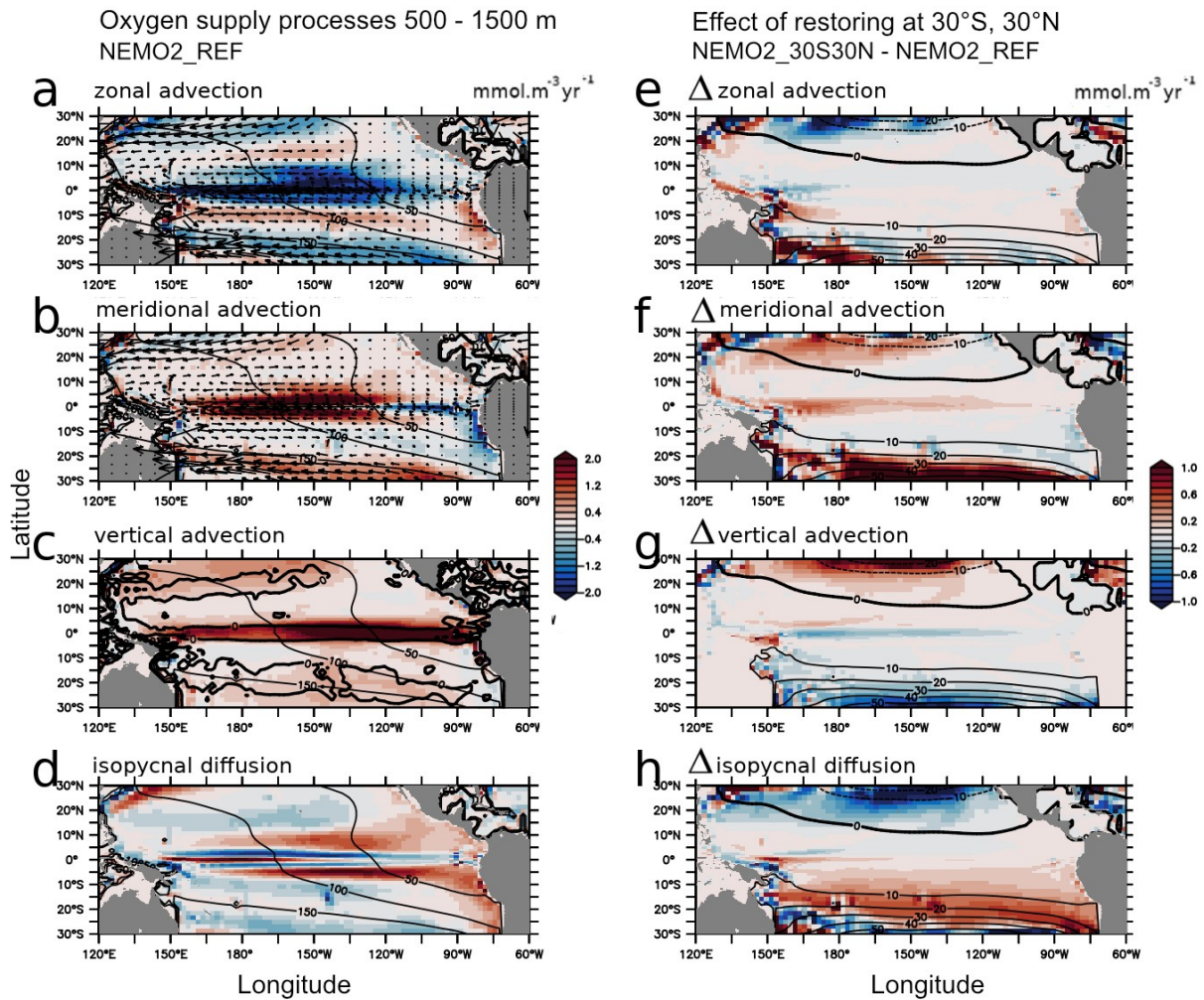
Figure 4 : a-d a Oxygen supply processes (mmol.m^{-3}.year^{-1} – average 500 - 1500m) in NEMO2_REF : a zonal advection, b meridional advection, c vertical advection, d isopycnal diffusion. The mean meridional and zonal currents are displayed as vectors (meridional, zonal advection). The mean vertical current (0 isoline) is represented as bold contour (vertical advection). Oxygen levels (mmol-m.$^{-3}$) are displayed in black contour. e-h: Difference in oxygen supply processes (mmol.m^{-3}.year^{-1} – average 500-1500m) between NEMO2_30S30N and NEMO2_REF : e- zonal advection, f- meridional advection, g- vertical advection, h- isopycnal diffusion. The NEMO2_30S30N – NEMO2_REF oxygen anomaly (mmol.m^{-3}) is displayed in contour.
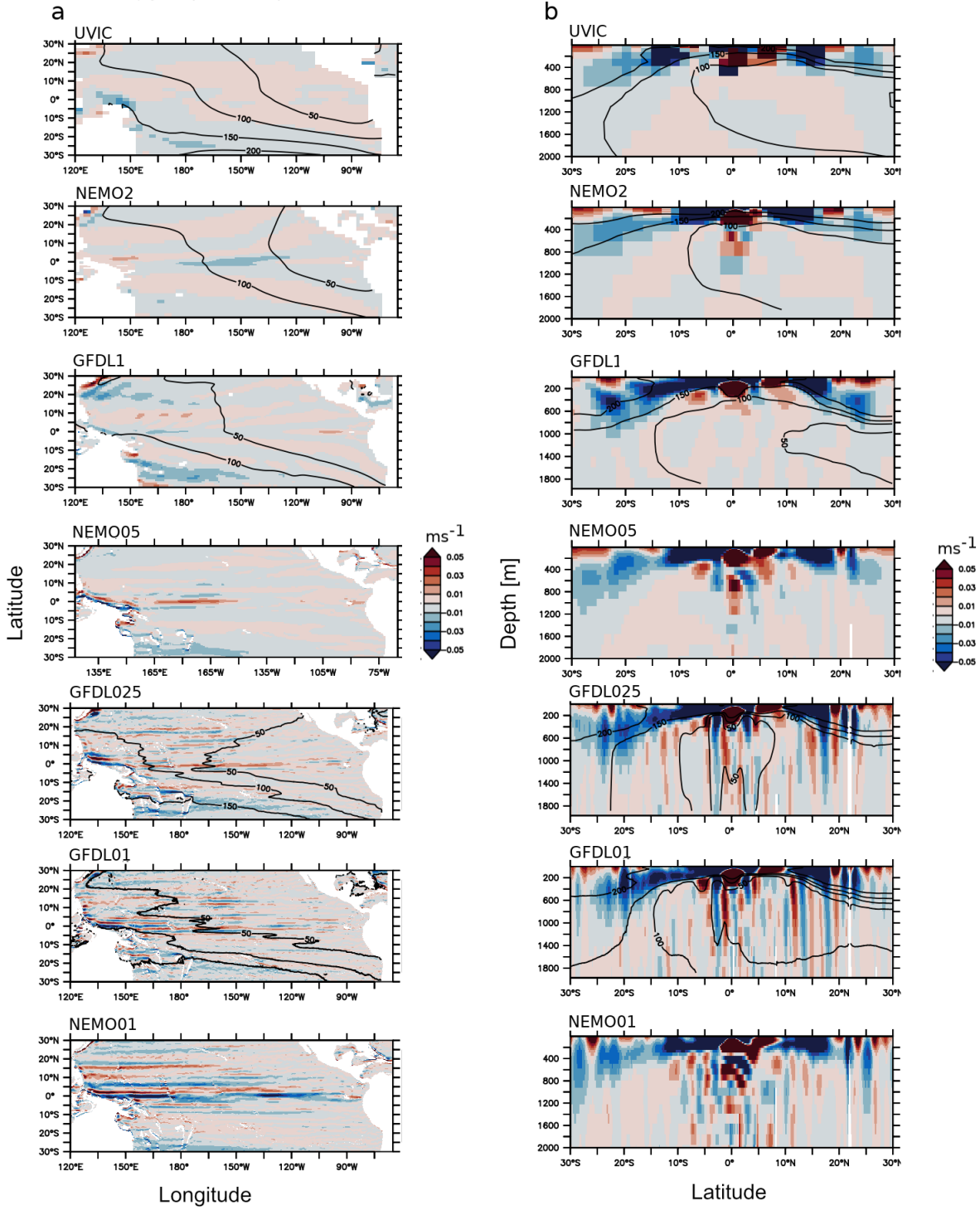
1047
1048 Figure 5 : mean currents velocity (ms⁻¹) at a- 1000 m depth b- 100°W in UVIC, NEMO2, NEMO05,
1049 GFDL025, GFDL01, NEMO01. The mean oxygen levels (mmol.m⁻³) (when coupled circulation-
1050 biogeochemical experiments have been performed – see Table 1) are displayed in contour.
1051
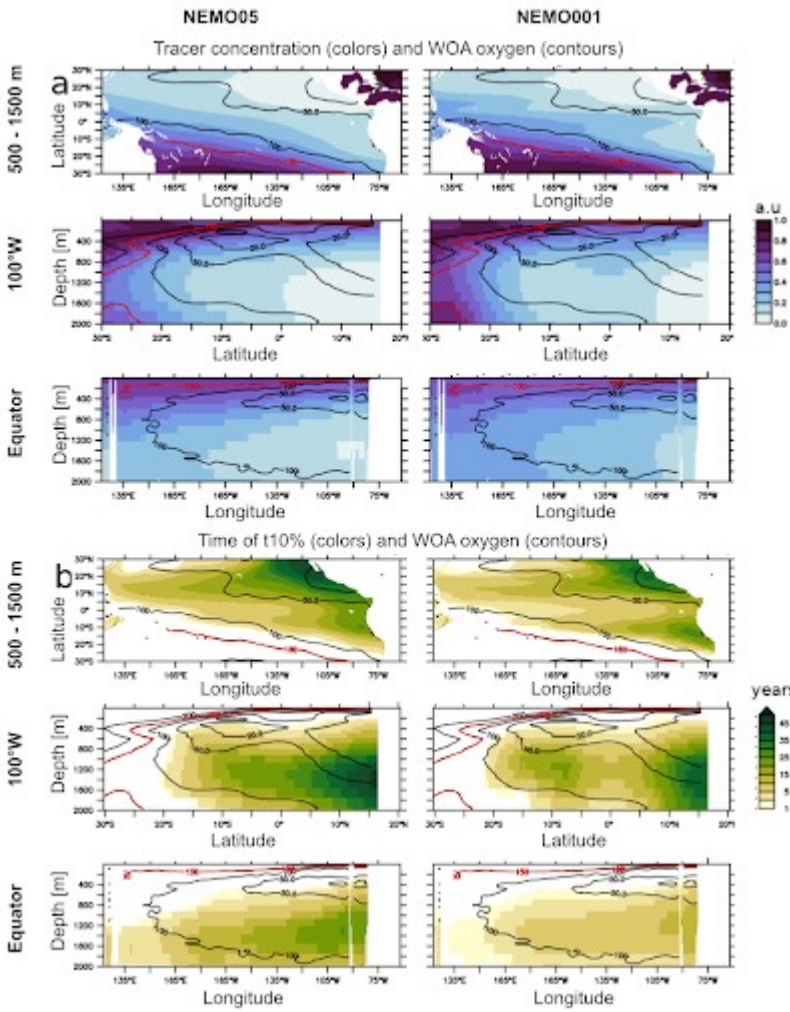
1052

1053 **[Fig above is replaced by Fig below]**

1054

1055
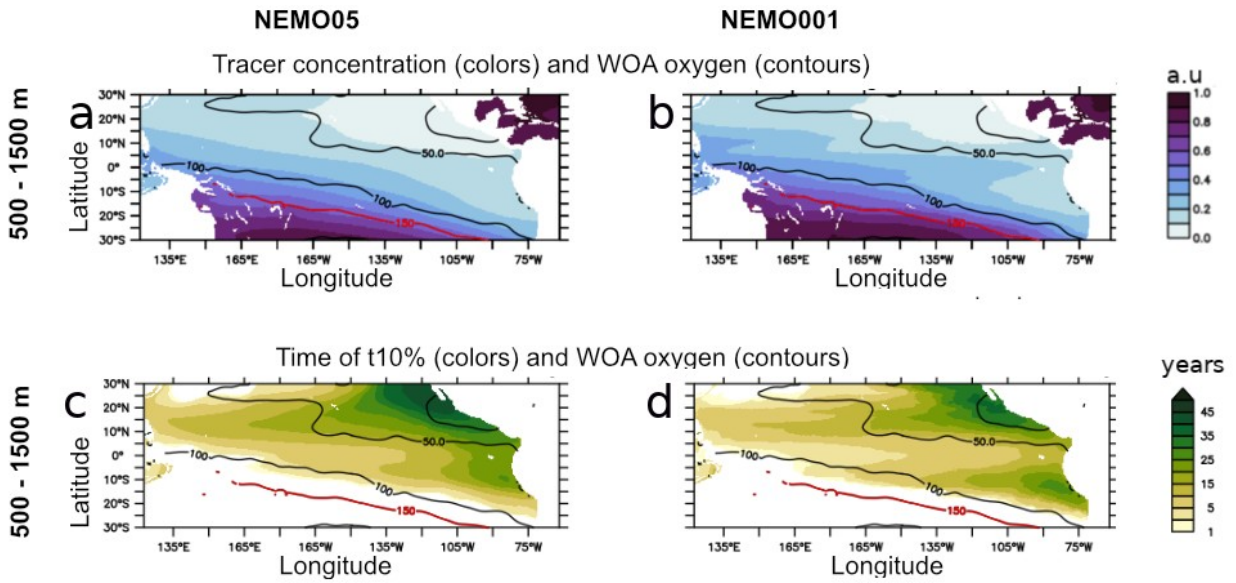
1056

Figure 6: ~~a :~~ mean 500 – 1500 m tracer concentration (arbitrary unit) after 60 years integration in a- NEMO05 and b - NEMO01 ~~: average 500-1500m, section 100°W, equatorial section~~. ~~b:~~ Time (years) at which the released tracer reaches the concentration 0.1 (t10%) in c- NEMO05 and d- NEMO01 ~~: average 500-1500m, section 100°W, equatorial section. In all the subpanels,~~ Tthe WOA oxygen levels (mean 500 – 1500 m) are displayed in contour. The red contour is the WOA 150 mmol.m^{-3} oxygen isoline, used to initialize the tracer level.
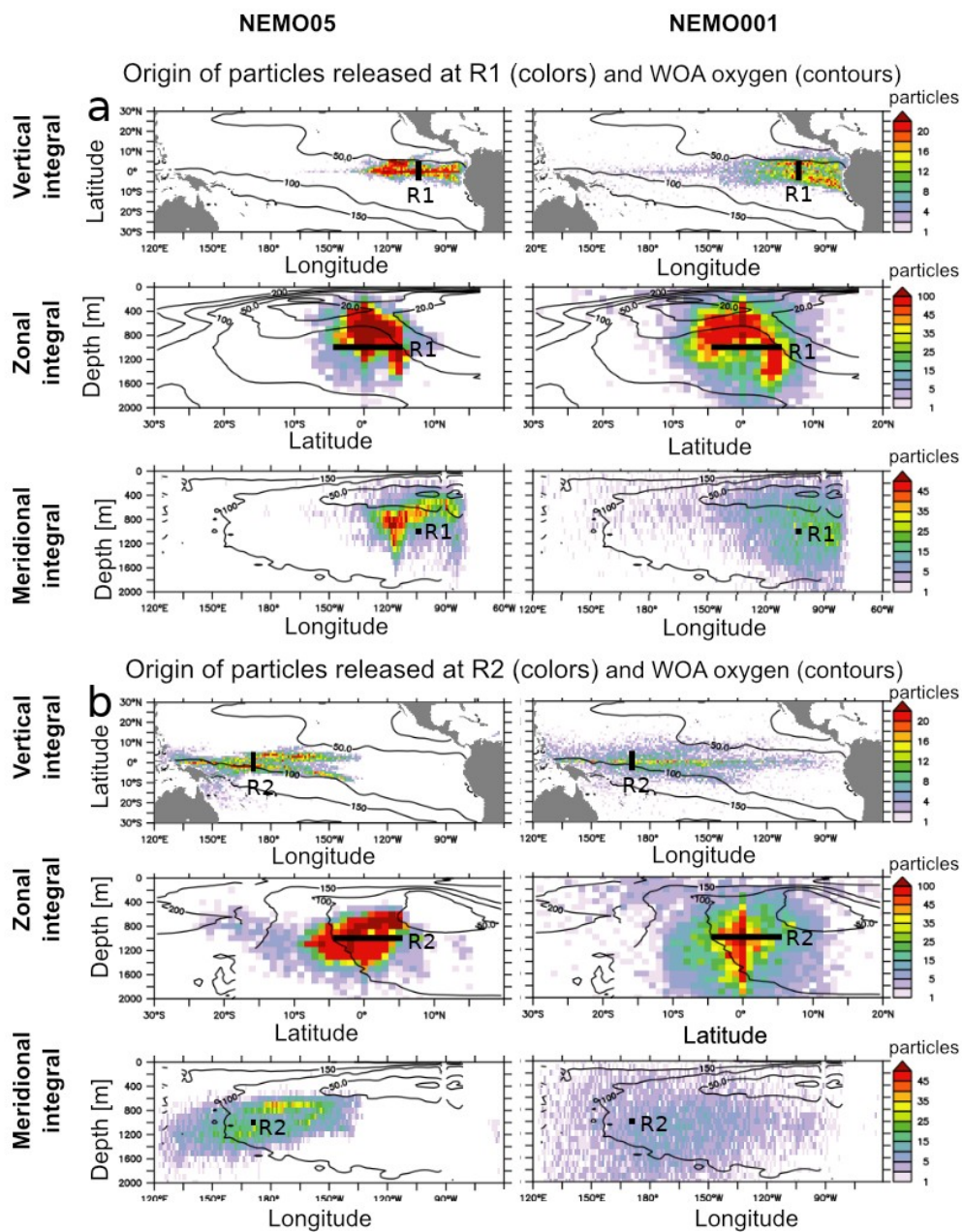
1066

1067 ~~Figure 7 : Density (number of particles in a 1°x1°x100m depth box) distribution of the location of~~
1068 ~~released Lagrangian particles (15 years backward integration starting from the final experiment~~
1069 ~~state) in NEMO05 and NEMO01. The release location is identified in bold and is located a- at~~
1070 ~~100°W/5°N-5S/1000 m depth (R1). b- at 160°E/5°N-5°S/1000 m depth (R2). The particles have~~
1071 ~~been integrated vertically, zonally and meridionally. The observed mean oxygen levels (WOA) are~~
1072 ~~displayed in contour.~~

1073 **[FIGURE DELETED]**

1074

1075
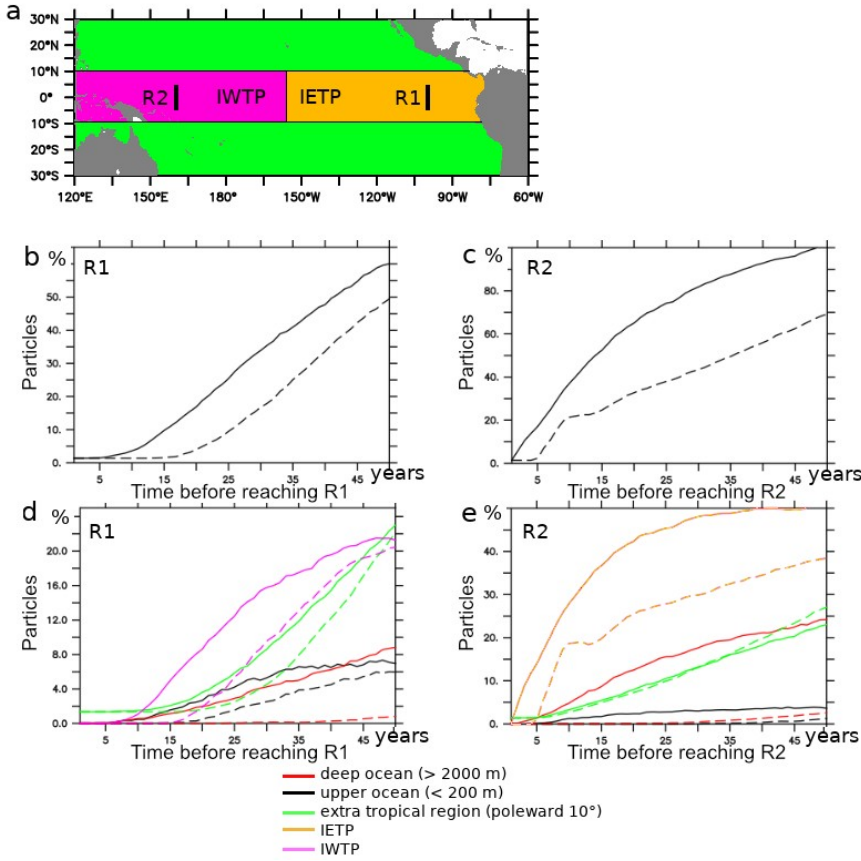
1076

1077 ~~Figure 8 : a- schema summarizing the releases (R1: 100°W / 5°N-5°S / 1000 m , R2: 160°E /~~
1078 ~~5N°5S / 1000 m) location, the IETP (Intermediate Eastern Tropical Pacific), IWTP (Intermediate~~
1079 ~~Western Tropical Pacific) regional extension. b. percentage of particles (release R1) originating~~
1080 ~~from outside the IETP ocean region. b- percentage of particles (release R2) originating from~~
1081 ~~outside the IWTP ocean region. d- percentage of particles (release R1) originating from the upper~~
1082 ~~ocean (shallower than 200 m), the deeper ocean (deeper than 2000 m), subtropical regions~~
1083 ~~(poleward 10°), the IWTP. e- percentage of particles (release R2) originating from the upper ocean~~
1084 ~~(shallower than 200 m), the deeper ocean (deeper than 2000 m), subtropical regions (poleward~~
1085 ~~10°), the IETP.~~

1086

1087 **[FIGURE DELETED]**

1088 Figure 7 and 8 have been replaced by 2 new figures (below)
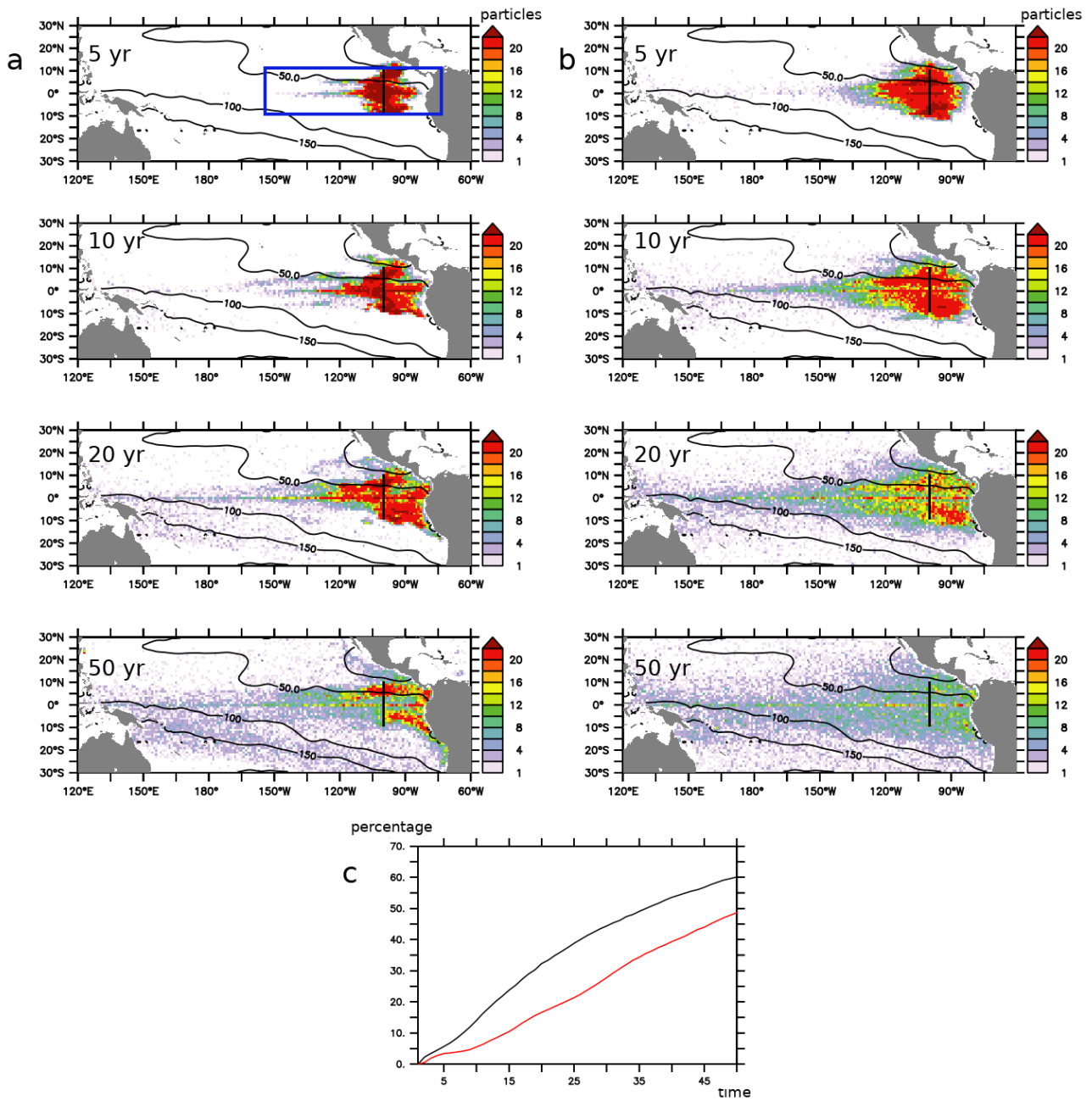
1089   Figure 7 : Density (number of particles in a 1°x1°x100m depth box) distribution of the location of
1090   released Lagrangian particles (backward integration in years) in a - NEMO05 and b- NEMO01. The
1091   release location is identified in bold and is located at 100°W/10°N-10S/500-1500 m depth (black
1092   line). The number of particles have been integrated vertically. The observed mean (500 – 1500 m)
1093   oxygen levels (WOA) are displayed in contour. The blue contour represents the Intermediate
1094   Eastern Tropical Pacific basin (IETP). c – percentage of particles originating outside the
1095   Intermediate Eastern Tropical Pacific (IETP) basin (160°W, 10°N-10°S, 500-1500 m) in NEMO05
1096   (red) and NEMO01 (black) over time (years)

1097
1098
1099
1100
1101
1102
1103
1104
1105
1106
1107
1108
1109
1110
1111
1112
1113
1114
1115
1116
1117
1118
1119
1120
1121
1122
1123
1124
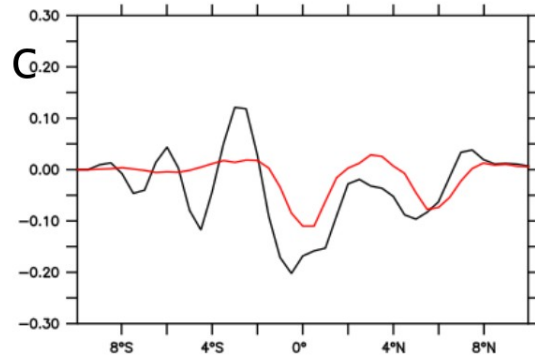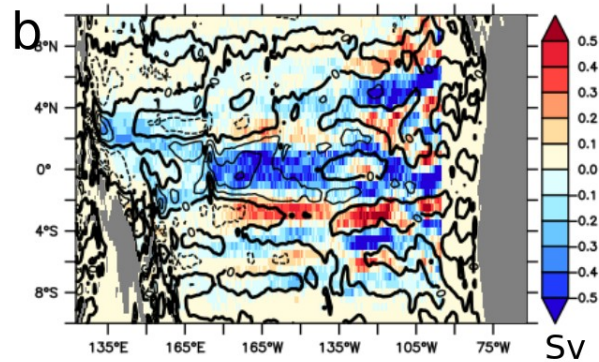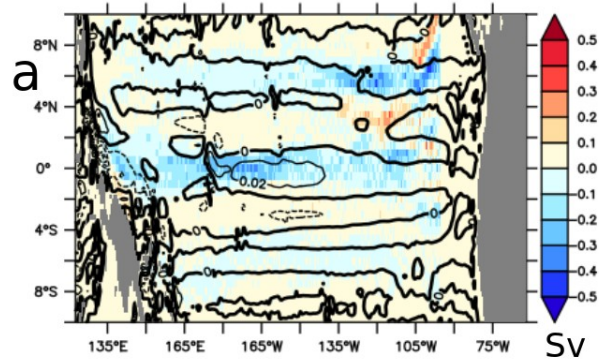
1125 Figure 8 : mean transport (Sv) in a- NEMO05 and -b NEMO01 derived from the release of particles
1126 at 100°W, 10°N-10°S, 500-1500m (backward integration). The mean zonal velocity (ms^{-1}) is
1127 represented in contour. c- zonally integrated transport (Sv) derived from the release of particles at
1128 100°W, 10°N-10°S, 500-1500m in NEMO05 (red) and NEMO01 (black)
1129
1130
1131
1132 Figure 9 : a - Mean Kinetic Energy (m2.s^{-2} x 1000) (average 10°N-10°S) in GFDL01, GFDL025,
1133 GFDL01, UVIC, b - similar to a. but average 160°W- coast. Oxygen levels (mmol.m^{-3}) are displayed

1142 Table 1 :

Model	Resolution	Atmosphere	Integration (years)	BGC	Model Reference (circulation)	Model Reference (BGC)
Mean state comparison						
UVIC	2.8°	Coupled (temperature, humidity) Forced (NCEP/ NCAR wind stress)	10000	UVIC-BGC	Weaver et al., 2001	Keller et al., 2012
NEMO2	2° (0.5 eq)	Forced COREv2 "normal year"	1000	NPZD-O2	Madec et al., 2015	Kriest et al, 2010 Duteil et al., 2014
GFDL1	1°	Coupled	190	BLING	Delworth et al, 2012, Griffies et al, 2015	Galbraith et al., 2015
GFDL025	0.25 °	Coupled	190	BLING		
GFDL01	0.1°	Coupled	190	BLING		
Process oriented experiments						
Model	Resolution	Atmosphere	Integration (years)	BGC	Characteristics	
NEMO2 -REF -30N30S -30N30S1500M (section 2.2.1)	2° (0.5 eq)	Forced COREv2 1948-2007	60	NPZD-O2	- control experiment - O2 restoring to WOA at 30°N/30°S - O2 restoring to WOA at 30°N/30°S/1500m	
NEMO05 (section 2.2.2)	0.5°	Forced COREv2 1948 - 2007	60	Tracer release	- Tracer initialized to 1 (O2 WOA > 150 mmol.m-3) or 0 (O2 WOA < 150 mmol-m-3)	
NEMO01 (section 2.2.2)	0.1°	Forced COREv2 1948 – 2007	60	Tracer release		

1143

1144

Annex A

The differences in oxygen levels between the "models groups" (GFDL suite, UVIC, NEMO2) are partly related to differences in the atmospheric fields employed and the integration time (see 2).

1. Wind forcing

Zonal wind mean stress typically varies by 5 to 20 % between the different wind products (Chauduri et al., 2013). To test this impact, we performed an experiment using the UVIC model using 2 different wind products (NCEP and COREv2 – Large and Yeager, 2009) (Figure A1). While the shape of the OMZ shows slight differences, the volume of the OMZ and the mean oxygen levels in the tropical regions and in the mid latitudes are similar. Consistent with the Figure 2, higher oxygen levels at 30°S lead to higher oxygen levels in the tropical ocean and to a smaller OMZ volume (Figure A2)
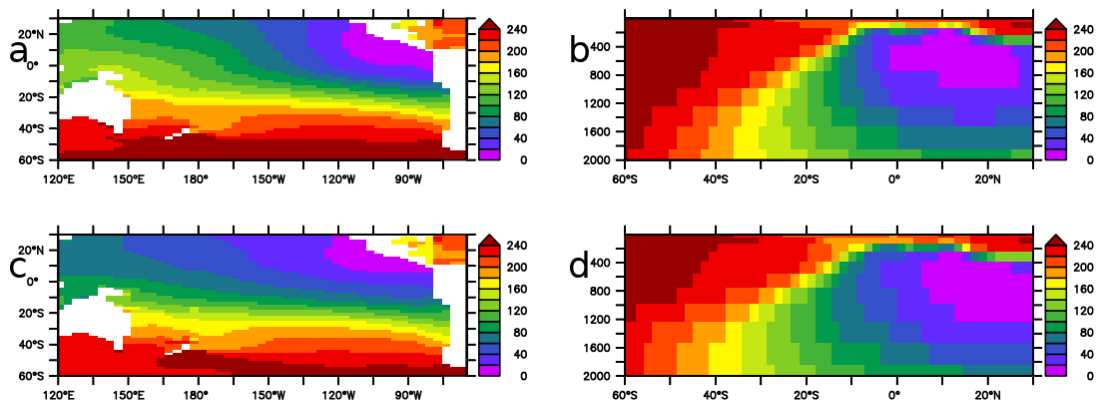
Figure A1 : Oxygen levels in UVIC (10000 years integration) a- mean 500-1500 m forcing NCEP. b- section 120°W forcing NCEP. c- mean 500-1500 m forcing COREv2, d- section 120°W forcing COREv2.
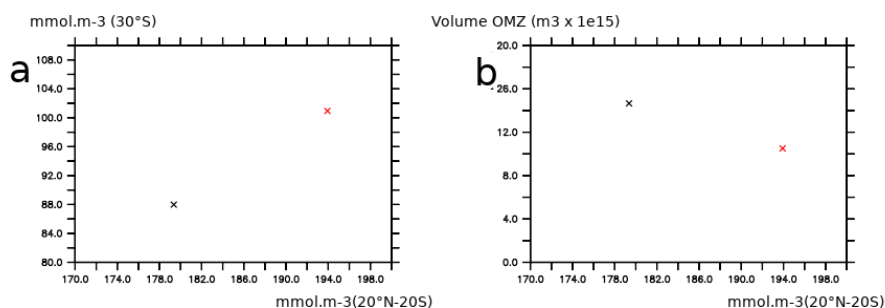
Figure A2 : a - Oxygen levels in UVIC (10000 years integration) at 30°S (zonal mean in the Pacific Ocean from surface to 2000 m depth) and in the tropical regions (20°S-20°N, averaged over the

whole Pacific Ocean). b - Oxygen levels in UVIC (10000 years integration) at 30°S (zonal mean in the Pacific Ocean, from surface to 2000 m depth) and volume of the OMZ in the Pacific Ocean. The configuration forced by COREv2 is shown in black, the configuration forced by NCEP is shown in red.

2. Spinup state

In complement, the spinup state of the model also impacts the oxygen levels as the deep ocean needs thousands of years to be in equilibrium. It may explain why UVIC (integrated for 10000 years) is characterized by much larger oxygen levels than the GFDL model suite (integrated for 190 years). As an example, the Figure A3 shows the evolution of oxygen levels during spinup in NEMO2. Larger oxygen levels at 30°S (e.g after 1000 years of integration) are characterized by a smaller OMZ volume (which is consistent with Fig 2) (Figure A4)
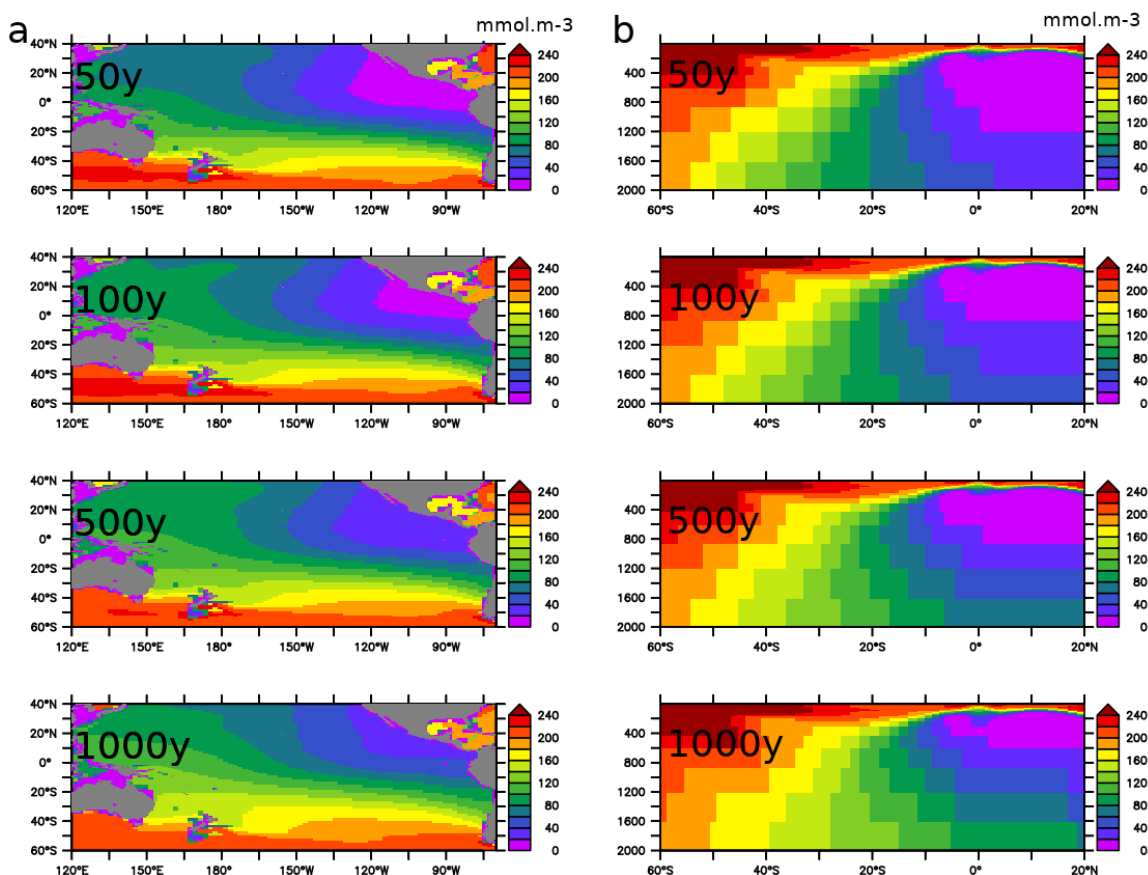
Figure A3 : oxygen levels at a - intermediate depth (average 500 – 2000 m) and b - 120°W in NEMO2 after 50, 100,500 and 1000 years integration
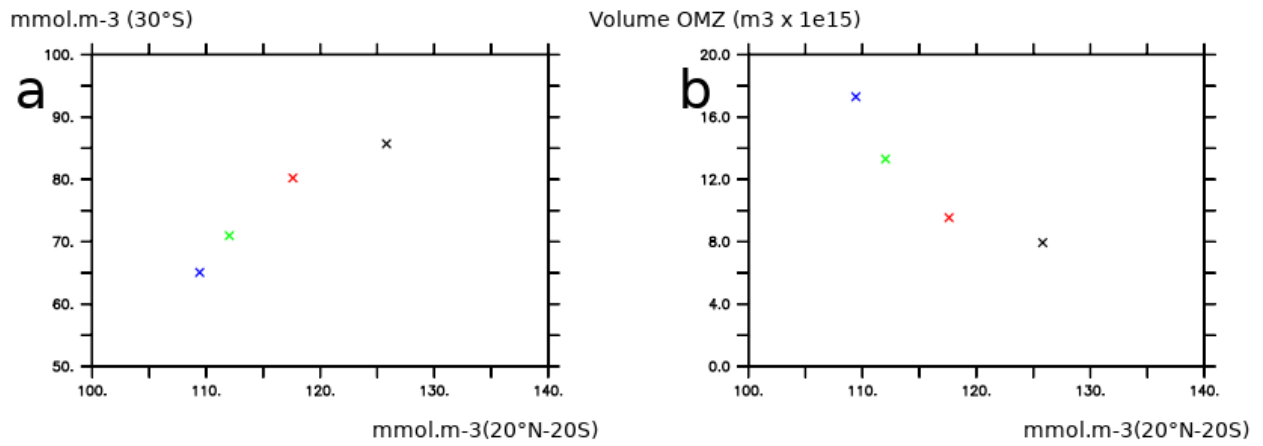
1199 Figure A4 : a - Oxygen levels in NEMO2 at 30°S (zonal mean in the Pacific Ocean from surface to
1200 2000 m depth) and in the tropical regions (20°S-20°N, averaged over the whole Pacific Ocean from
1201 surface to 2000 m depth). b - Oxygen levels in NEMO2 at 30°S (zonal mean in the Pacific Ocean
1202 from surface to 2000 m depth) and volume of the OMZ in the Pacific Ocean. The color of the cross
1203 depends of the integration duration (black : 50 years, red : 100 years, green : 500 years, blue 1000
1204 years).
1205
1206
1207
1208
1209
1210
1211
1212
1213
1214
1215
1216
1217
1218
1219
1220
1221
1222
1223
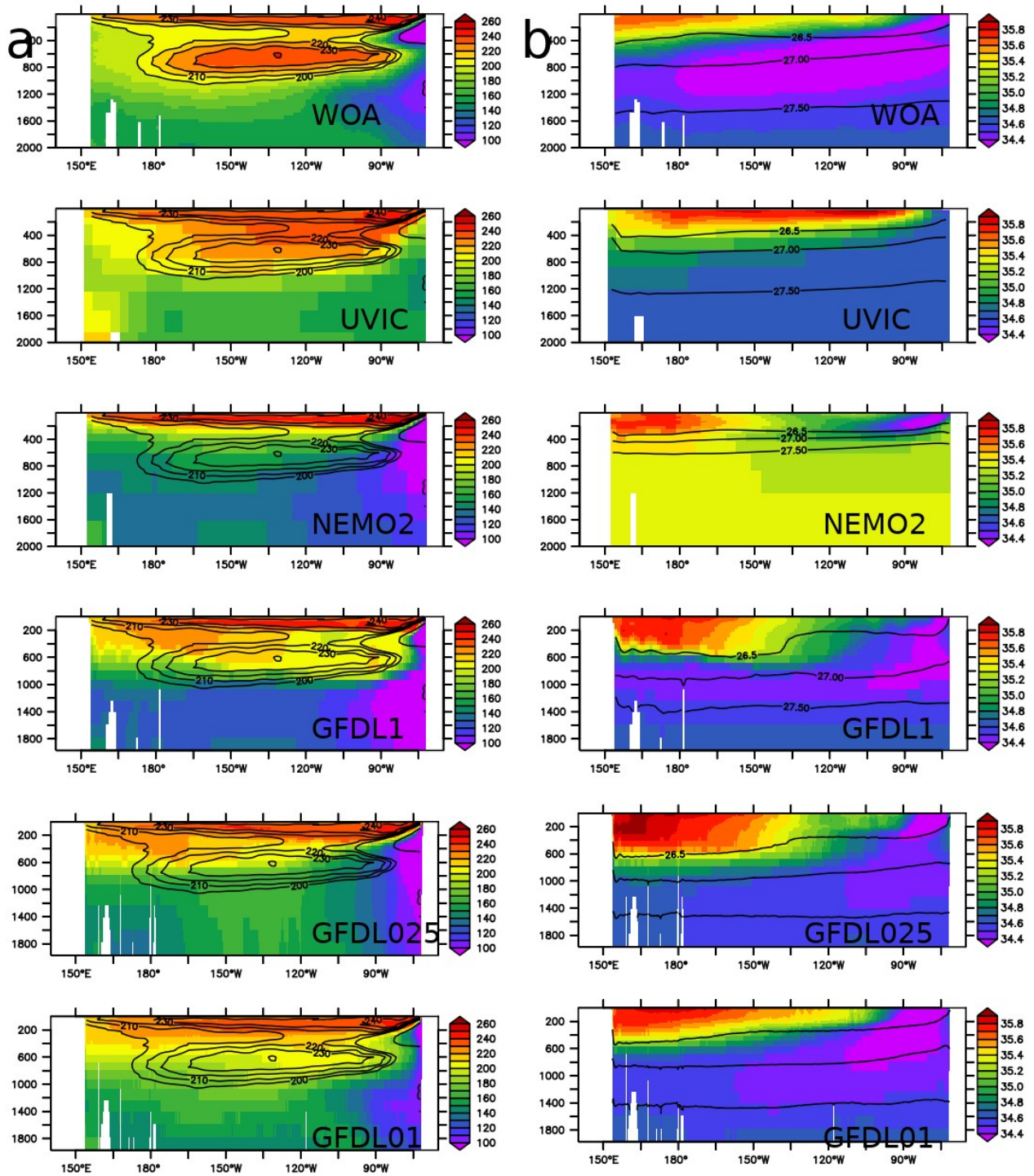
1224
1225 Figure A5 : a - oxygen levels (mmol.m-3) in observations and models at 30°S. The WOA oxygen
1226 levels are displayed in contour. b- salinity in observations and models at 30°S. The density
1227 anomaly (26.5, 27, 27.5) is displayed in contour.

1228
1229
1230
1231

1232 References

1233 Chaudhuri, Ayan & Ponte, Rui & Forget, Gael & Heimbach, Patrick. (2013). A Comparison of

1234 Atmospheric Reanalysis Surface Products over the Ocean and Implications for Uncertainties in Air-

1235 Sea Boundary Forcing. Journal of Climate. 26. 153-170. 10.1175/JCLI-D-12-00090.1.

1236 Large, W.G., Yeager, S.G. (2009). The global climatology of an interannually varying air–sea flux

1237 data set. Clim Dyn 33, 341–364. 10.1007/s00382-008-0441-3

1238

1239

1240 **Annex B**

1241 The deficiency in oxygen in NEMO2-REF is clearly highlighted at 30°S, between 400 and 1500m.

1242 In comparison, the density field is well represented in NEMO2-REF. At 500m, density is about 26.6

1243 in both WOA and NEMO2-REF. At 1500 m , the density is 27.6 in WOA and only 27.4 in NEMO2-

1244 REF, highlighting some potential water mass formation issue in NEMO2, as in most of models. A

1245 section at 100°W shows that isopycnal are almost horizontal at intermediate depth (500 – 1500 m)

1246 in WOA and NEMO2 in the subtropical and tropical ocean.

1247

1248
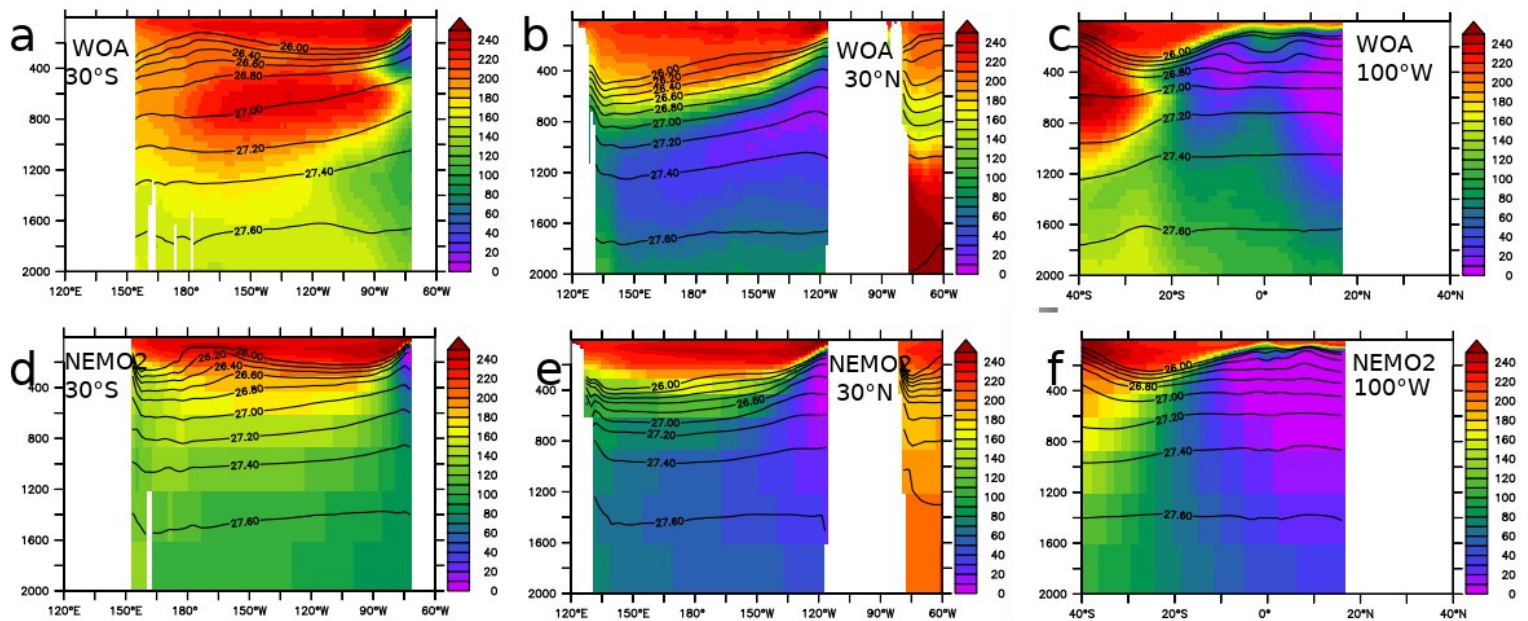
1249 Fig B1 : oxygen levels (mmol.m^{-3}) (color) and density levels (contour) at 30°S, 30N and 100°W in

1250 the WOA dataset (a,b,c) and NEMO2-REF experiment (d,e,f)

1251

1252

1253 Annex C

The experiments discussed in 4.2 were not coupled with biogeochemical cycles for computational cost reasons. In order to assess the robustness of our findings (EICS plays a large role in setting tropical oxygen levels), we next analyze equatorial oxygen in a set of climate models similar to CMIP models. To this end we use the GFDL model suite, characterized by a resolution increase (GFDL1, GFDL025 and GFDL01 - see Table 1).

The striking difference between GFDL01 and GFDL025 / GFDL1 are the high oxygen levels in the eastern part of the ocean below 1000 m in GFDL01 compared to GFDL025/GFDL1 (Fig 2). The oxygen levels show weaker zonal gradient in GFDL01, consistent with the tracer experiment that we performed in 4.2. and a more ventilated intermediate equatorial ocean. High values of mean kinetic energy are associated with higher oxygen values (Fig C1). This is particularly clear in GFDL01 at around 1500 m depth, where strong values of MKE are present and form the "bottom" of the low oxygen volume (oxygen lower than 50 mmol.m-3). Conversely GFDL025 and GFDL1 do not present high MKE values below 1000 m in the eastern part of the basin; the low oxygen volume extends till depths greater than 2000 m. It suggests that intermediate currents participate in the ventilation of the eastern tropical ocean and thus in limiting the vertical extension of the OMZ.

Oxygen levels do not increase linearly with the currents strength, i.e while currents strength increase in GFDL1, GFDL025 and GFDL01, oxygen levels are relatively similar in GFDL1 and GFDL025 (see Fig 5 and Fig C1). The relatively small net balance between large fluxes of respiration and oxygen supply (Duteil et al., 2014) may be responsible for this behavior. If the supply is slightly higher compared to the consumption by respiration, it will lead to an increase of oxygen concentration. If it is slightly lower, the oxygen levels will decrease. A small difference in supply (e.g slightly weaker currents) may therefore lead to a large difference in oxygen levels when integrated over decades. For this reason, the impact of the EICS is more visible below 1000 m as the respiration decreases following a power-law with depth (Martin et al., 1987) and is therefore easier to offset even by a moderate oxygen supply.

Resolving explicitly the EICS results in a similar oxygen distribution to what Getzlaff and Dietze (2013) (GD13) achieved with a simple EICS parameterization (Fig C1a): to compensate for the "missing" EICS in UVIC, a coarse resolution model, they enhanced anisotropically the lateral diffusivity in the equatorial region. The oxygen levels from UVIC GD13 are shown in blue contours on top of the UVIC oxygen distribution (black) in Fig C1. Implementing this approach tends to homogenize oxygen levels zonally, with an increase of the mean levels by 30-50 mmol.m-3 in the eastern basin and a decrease of oxygen concentrations in the western basin. While this approach may be useful to better represent the oxygen mean state, it however does not take into account the potential variability and future evolution of the EICS.

Mean kinetic energy

Average 10°N - 10°S (colors) and oxygen (contours)

Average 60°W - coast (colors) and oxygen (contours)
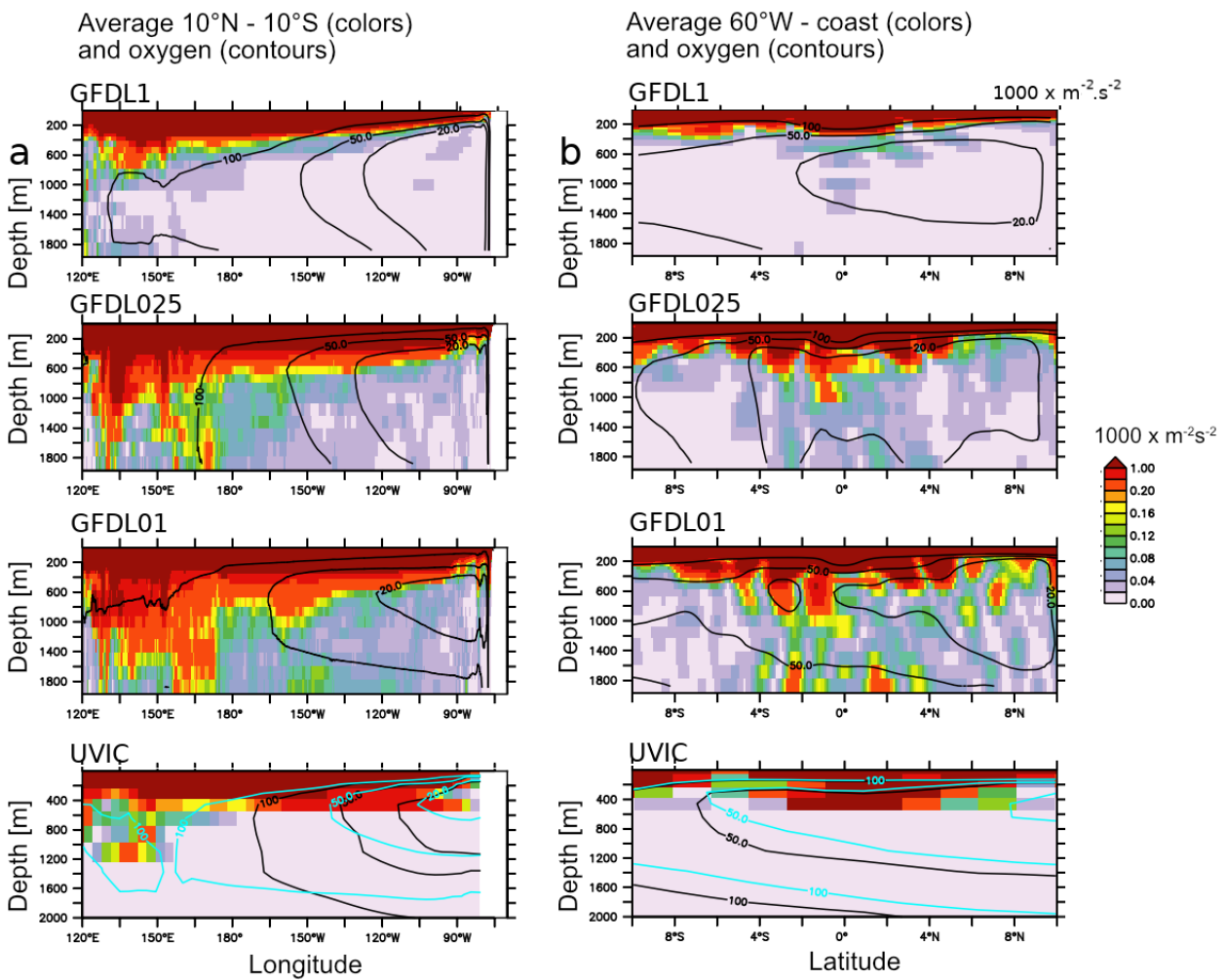
Figure C1 : a - Mean Kinetic Energy (m2.s-2 x 1000) (average 10°N-10°S) in GFDL01, GFDL025, GFDL01, UVIC, b - similar to a. but average 160°W- coast. Oxygen levels (mmol.m-3) are displayed in black contour. The blue contour corresponds to UVIC GD13 (Getzlaff and Dietze, 2013, including an anisotropical increase of lateral diffusion at the equator)